

QUANTUM NOISE & ACTUATOR BASED CONTROL IN SPIN ENSEMBLES



A thesis submitted towards partial fulfilment of
BS-MS Dual Degree Programme

by

GOVIND UNNIKRISHNAN

under the guidance of

DR TS MAHESH

IISER PUNE

INDIAN INSTITUTE OF SCIENCE EDUCATION AND RESEARCH
PUNE

Certificate

This is to certify that this thesis entitled "Quantum Noise & Actuator Based Control in Spin Ensembles" submitted towards the partial fulfilment of the BS-MS dual degree programme at the Indian Institute of Science Education and Research Pune represents original research carried out by Govind Unnikrishnan at Indian Institute of Science Education and Research, Pune, under the supervision of Dr TS Mahesh during the academic year 2015-2016.



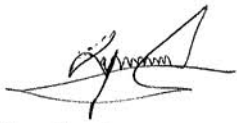
Student
GOVIND UNNIKRIISHNAN



Supervisor
DR TS MAHESH

Declaration

I hereby declare that the matter embodied in the report entitled “Quantum Noise & Actuator Based Control in Spin Ensembles” are the results of the investigations carried out by me at the Department of Physics, Indian Institute of Science Education and Research, Pune, under the supervision of Dr TS Mahesh and the same has not been submitted elsewhere for any other degree.



Student
GOVIND UNNIKRISHNAN



Supervisor
DR TS MAHESH

Acknowledgements

First and foremost, I express my heartfelt gratitude to Dr TS Mahesh for his guidance. I also thank Deepak Khurana for his camaraderie during this project and Abhishek Shukla for helping us with the spectrometer in times of need. Finally, without getting into literary hyperboles, I would simply like to acknowledge the support given to me by all my friends and family.

Abstract

This thesis is divided into three parts. In the first part, the protection offered by decoherence free subspaces is quantified and compared against unprotected spaces by means of noise spectroscopy. In the second part, decoherence is studied in two kinds of engineered systems, one model for phase decoherence and the other for spin flip decoherence. In both models, the combination of two noise sources viz. stochastic kicks and temporally randomized flip operations, is shown to lead to frustration of decoherence under certain resonant conditions. Finally, in the third part, the realization of a universal set of gates on a spectroscopically indistinguishable pair of nuclear spins is demonstrated, facilitating improved decoherence free subspaces.

Contents

| | | |
|----------|---|-----------|
| 1 | Introduction | 4 |
| 1.1 | Decoherence Suppression: An overview | 5 |
| 1.1.1 | Dynamical Decoupling | 5 |
| 1.1.2 | Decoherence Free Subspaces | 6 |
| 1.2 | Thesis Outline | 7 |
| 2 | Noise Spectroscopy in a Decoherence Free Subspace | 8 |
| 2.1 | Noise Spectroscopy | 8 |
| 2.2 | Experimental Implementation | 9 |
| 2.2.1 | Long Lived Coherences | 9 |
| 2.2.2 | Measuring Noise Spectrum | 12 |
| 2.3 | Results | 13 |
| 2.4 | Conclusion and Discussion | 15 |
| 3 | Frustrated Decoherence | 17 |
| 3.1 | Engineered Decoherence | 17 |
| 3.1.1 | Stochastic Kick Method | 17 |
| 3.1.2 | Kondo's method | 20 |
| 3.1.3 | Spin Flip Decoherence | 21 |
| 3.2 | Combining the two methods of engineered decoherence | 23 |
| 3.2.1 | Phase damping model | 23 |
| 3.2.2 | Spin flip model | 24 |
| 3.2.3 | Bloch Sphere Distortions | 24 |
| 3.3 | Results | 24 |
| 3.3.1 | Dephasing Model | 24 |
| 3.3.2 | Spin flip Model | 32 |
| 3.4 | Conclusion and Discussion | 35 |
| 4 | Quantum Control in Equivalent Spins | 37 |
| 4.1 | Qubits and the Bloch Sphere | 37 |
| 4.2 | Quantum Control | 38 |

| | | |
|-------|--|-----------|
| 4.2.1 | Lie Algebras and Lie Groups | 38 |
| 4.2.2 | Controllability | 39 |
| 4.2.3 | Basis of a dynamical Lie Algebra | 40 |
| 4.2.4 | Quantum Control in Deoherence Free Subspaces | 40 |
| 4.2.5 | Actuator Based Quantum Control | 41 |
| 4.3 | Experimental Implementation | 41 |
| 4.3.1 | Universal Gates | 42 |
| 4.3.2 | Suppressing Superfluous Signals | 44 |
| 4.4 | Results | 47 |
| 4.4.1 | CNOT gate | 47 |
| 4.4.2 | Hadamard gate | 48 |
| 4.4.3 | $\pi/8$ gate | 50 |
| 4.5 | Conclusion and Discussion | 52 |
| | References | 53 |

Chapter 1

Introduction

The dawn of quantum theory in the 1900s introduced a paradigm shift in our perspective of the physical universe. Notions such as superposition of states and entanglement were, and continue to be, extremely counterintuitive and led to both physical and philosophical dilemmas, the most famous of them being the Einstein-Podolsky-Rosen (EPR) [1] paradox and the Schrödinger's cat paradox [2]. During the initial years, experiments confirming quantum theory were confined to the microscopic realm, so much that some were of the opinion that there is a distinct dichotomy between theories describing the classical world of everyday experience and the strange, non-intuitive microscopic realm where quantum mechanics reigned supreme. However, as time progressed, quantum mechanical phenomena such as interference has been demonstrated in the macroscopic limit as well. For instance, a landmark paper was published where C_{60} fullerene molecules were demonstrated to produce an interference pattern in a double slit experiment [3].

Despite the observation of quantum mechanical phenomena in macroscopic physics, the boundary between the quantum and classical world was still relatively blurred, giving rise to much research on the quantum-to-classical transition. How does a quantum mechanical phenomenon like interference mysteriously disappear as one approaches the classical world? The solution to this stemmed from the realization that one had rather hastily carried over the notion of *locality* from classical physics to quantum theory [4]. In classical physics, we often assume that a system (say a cricket ball) preserves all its prior properties after an interaction with an environment (such as a collisions with air molecules) and can be analyzed independently after the event of an interaction. However, in the quantum realm, an interaction leads to the system and environmental states to become *entangled* i.e. in simple terms, neither of them can be described independently (locally) after the interaction, even if they are spatially well separated. This interaction

with the environment also leads to an irreversible dispersion of *quantum coherence*, the relative phase information between different quantum states of the system, to the entangled system-environment state, thus taking it out of our field of observation[4]. This irreversible loss of quantum coherence from the system of interest, which also explains the absence of quantum phenomena in the general macroscopic, interaction prone world, is generally termed as decoherence.

Although the study of decoherence phenomena is an interesting topic in itself, having implications to fundamental problems in physics, the emergence of quantum information science has accelerated research in this field. In quantum information science, we utilize quantum phenomena such as interference and entanglement to perform tasks much more efficiently than a classical computer can ever achieve. The classic example for this is the difficult problem of efficiently finding prime factors of a number, something which is crucial to existing cryptography protocols. While the time for prime factorization on a classical computer scales exponentially with input size, Peter Shor gave a quantum algorithm which runs in polynomial time [5]. Another quantum algorithm is Grover's search algorithm [6] which performs with $O(\sqrt{N})$ complexity whereas the classical counterpart has $O(N)$ complexity. Although the prospect of a large scale quantum computer promises to open up a multitude of possibilities, the physical realization of such systems are laden with difficulties, the most severe of them being decoherence. In order to utilize quantum mechanical properties, one needs to preserve the quantum coherence between states, a task which becomes exceedingly difficult as one scales up from the microscopic domain due to increased decoherence.

1.1 Decoherence Suppression: An overview

Decoherence is a persistent problem in quantum information science, irrespective of the physical system chosen to represent the qubit. Various methods have been adopted to counter decoherence-dynamical decoupling [7, 8], quantum error correcting codes [9], and decoherence free subspaces[10] being some of them. Here, we deal with dynamical decoupling and decoherence free subspaces.

1.1.1 Dynamical Decoupling

A dynamical decoupling (DD) sequence is a series of equidistant flip operations on the system qubit. Each flip operation reverses the 'direction' of evolution of the qubit, effectively keeping the system from evolving under

the noise operator. This is a very common method employed in NMR experiments, where magnetic field inhomogeneities often cause nuclear spins to precess at different frequencies leading to a loss of signal.

1.1.2 Decoherence Free Subspaces

While DD is an active suppression technique, decoherence free subspaces achieve noise suppression by utilizing certain symmetry properties inherent in the encoding. The idea is to create logical qubits using two or more physical qubits such that the effect of noise gets nullified. For instance, say we encode a logical qubit as follows:

$$|0\rangle_L = \frac{|01\rangle + |10\rangle}{\sqrt{2}}, |1\rangle_L = \frac{|01\rangle - |10\rangle}{\sqrt{2}}$$

For an interaction of the type ,

$$H_{int} = J\sigma_z^1\sigma_z^2$$

between the two qubits which compose the logical qubit, since $|0\rangle$ and $|1\rangle$ are eigenstates of the Pauli operator σ_z , we have

$$\sigma_z |0\rangle = |0\rangle$$

$$\sigma_z |1\rangle = -|1\rangle$$

Therefore, when the interaction Hamiltonian H_{int} acts on the states $|0\rangle_L$ and $|1\rangle_L$ at any time t , the phases accumulated by $|0\rangle$ and $|1\rangle$ cancel each other:

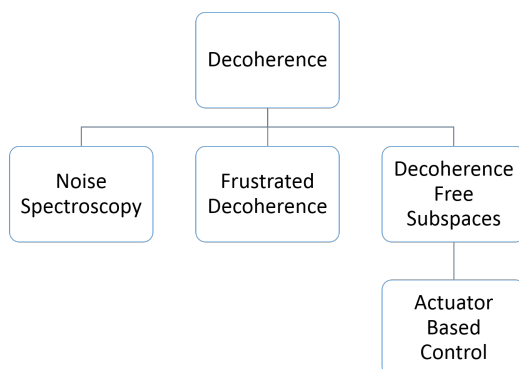
$$\begin{aligned} e^{-iH_{int}t} |01\rangle &= e^{-iJ\sigma_z^1\sigma_z^2t} |01\rangle \\ &= e^{-iJ\sigma_z^1I^2t} |0\rangle e^{-iI^1\sigma_z^2t} |1\rangle \\ &= e^{-iJt} |0\rangle e^{+iJt} |1\rangle = |01\rangle \end{aligned}$$

Hence, we say that the subspace spanned by $|0\rangle_L$ and $|1\rangle_L$ is a *decoherence free subspace*.

1.2 Thesis Outline

Oftentimes, an attempt to protect the system by isolating it from external decohering influences also compromises the degree of control one has over the system. Furthermore, although it has been shown that many techniques will suppress decoherence, before one envisions a large scale quantum computer, it is necessary to quantify and characterize the decoherence processes which are relevant to the qubits in question. A better understanding of the dynamics and characteristics of decoherence processes will enable one to fine tune existing techniques while opening up possibilities of novel suppression techniques. However, this requires the study of decoherence in a controlled manner, which is often not possible in natural systems.

In this thesis, we tackle the issues mentioned above. Firstly, the performance of decoherence free subspaces is characterized using noise spectroscopy and compared against unprotected qubits. Secondly, besides the existing experimentally feasible model for phase decoherence [11], a model for amplitude damping from our previous work is presented. Both kinds of engineered decoherence processes are studied under the simultaneous action of two noise sources, leading to a ‘frustration’ of decoherence under certain resonant conditions [12]. Finally, we demonstrate how one may achieve universal control in a two qubit system while simultaneously protecting it from noise, namely by utilizing a decoherence free subspace (DFS) composed of effectively indistinguishable nuclear spins. Previous work [13] shows that a full return to the DFS after state manipulation is not possible unless the spins are chemically indistinguishable, whereas the use of indistinguishable spins would mean the loss of universal control over the system. Our method, which utilizes the anisotropic couplings between nuclear spins to effect quantum gates, circumvents this quandary. The figure below summarizes how this thesis is organized.



Chapter 2

Noise Spectroscopy in a Decoherence Free Subspace

Before we explain noise spectral density in the context of decoherence free subspaces, we first describe the concept itself.

2.1 Noise Spectroscopy

Information regarding the characteristics of noise in a quantum system will be beneficial in improving existing noise suppression techniques and developing new ones. An important technique which gives the spectral distribution of noise is noise spectroscopy. In general, for a time series $x(t)$, a power spectrum gives the distribution of the variance of $x(t)$ over the frequency domain. Correspondingly, the power spectral density gives the rate of variance contributed by frequencies in the immediate neighborhood of a frequency f , to the variance of $x(t)$ per unit frequency. Formally, we define the power spectral density as the Fourier transform of the autocorrelation function.

Yuge *et al* [14] have described how to measure the dephasing noise spectrum of a single qubit attached to an environmental bath. The method involves the use of a series of equidistant π pulses (a Carr-Purcell-Meiboom-Gill or CPMG sequence) to the system qubit (schematically shown in Fig. 2.1). They have shown that at a frequency $\omega = \frac{\pi}{2\tau}$, the spectral density is given as [14]:

$$S(\omega) \approx \frac{\pi^2}{4T_2} \tag{2.1}$$

where T_2 is the spin-spin relaxation time under the application of a CPMG sequence at a frequency $\omega = \frac{\pi}{2\tau}$.

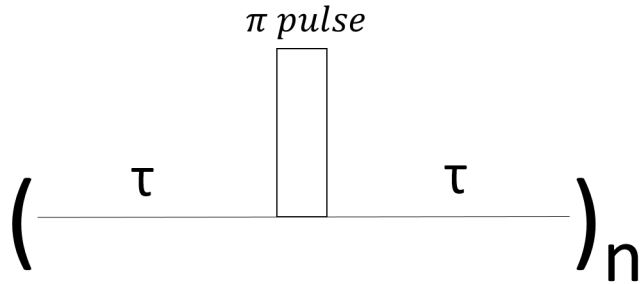


Figure 2.1: A CPMG sequence with the delay between π pulses equal to 2τ

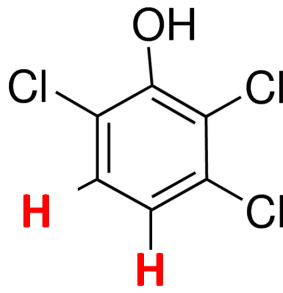


Figure 2.2: Structure of 2,3,6-trichlorophenol. Red Hs are the spins used as qubits

2.2 Experimental Implementation

To measure the noise spectrum, we chose the two qubit system 2,3,6-trichlorophenol (see Fig. 2.2). 7.21mg of the compound was dissolved in 600 μL of dimethyl sulfoxide- d_6 (DMSO- D_6). Before describing how the noise spectral density of a decoherence free subspace was measured, we introduce the concept of long lived coherences in NMR.

2.2.1 Long Lived Coherences

First, we write down the general two qubit Hamiltonian with a scalar coupling constant J_{IS} , where the I and S label the two qubits [15](setting $\hbar=1$):

$$\mathcal{H} = \nu_I I_z + \nu_S S_z + J_{IS} \vec{I} \cdot \vec{S} \quad (2.2)$$

where the term $J_{IS} \vec{I} \cdot \vec{S}$ describes the magnetic interaction between the two qubits. For a weakly coupled system ($\Delta\nu = \nu_I - \nu_S \gg |J|$), we may neglect

the xx and yy products of Pauli operators from $\vec{I} \cdot \vec{S}$

$$\mathcal{H} = \nu_I I_z + \nu_S S_z + J_{IS} I_z S_z \quad (2.3)$$

The eigenbasis of 2.3 is given by the product basis $\{|\alpha\alpha\rangle, |\alpha\beta\rangle, |\beta\alpha\rangle, |\beta\beta\rangle\}$ where $|\alpha\rangle, |\beta\rangle$ take on the values $|\pm\frac{1}{2}\rangle$ or $|0, 1\rangle$ in qubit notation. In the absence of a magnetic field, the two states become degenerate or in other words, equivalent. In this situation, the Hamiltonian may be written as

$$\mathcal{H} = J_{IS} \vec{I} \cdot \vec{S} \quad (2.4)$$

with an eigenbasis defined by singlet and triplet states [15]:

$$|T_0\rangle = \frac{1}{\sqrt{2}}(|01\rangle + |10\rangle) \quad (2.5)$$

$$|T_{+1}\rangle = |00\rangle \quad (2.6)$$

$$|T_{-1}\rangle = |11\rangle \quad (2.7)$$

$$|S_0\rangle = \frac{1}{\sqrt{2}}(|01\rangle - |10\rangle) \quad (2.8)$$

$$(2.9)$$

Sarkar *et al* [15] defines a long lives coherence as a superposition between the singlet and zero quantum triplet states:

$$\rho_{LLC} = |S_0\rangle \langle T_0| + |T_0\rangle \langle S_0| \quad (2.10)$$

Now, we note that both $|S_0\rangle$ and $|T_0\rangle$ defined by 2.8 and 2.5 belong to the decoherence free subspace defined in Sec. 1.1.2. Sarkar *et al* have shown that if we transform the state defined by $I_x - S_x$ in the product basis to the singlet triplet basis, we will reach LLC state defined in 2.10. Physically, this corresponds to making the spins degenerate once again by removing the effect of the magnetic field. In practice, this is achieved by using the technique of **spin lock**.

Spin lock is a technique used to nullify the effect of the main magnetic field in NMR. When two spins are precessing at different precession frequencies (chemical shifts) about the main field, the application of a strong RF field having the same phase as the magnetization along another axis will suppress the differential precession between the spins, making them chemically equivalent [16]. For example, we may flip the magnetization from the longitudinal direction (z-axis) to the transverse direction (x-axis) and then apply a strong RF field along the x-axis as shown in Fig. 2.3:

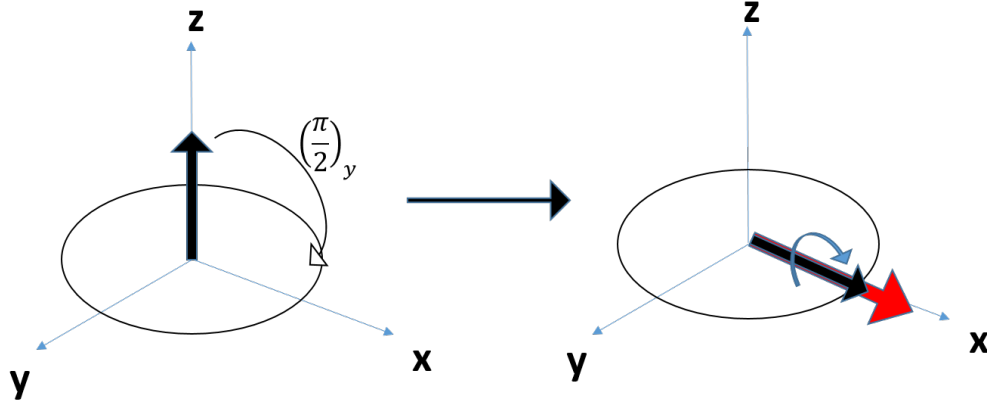


Figure 2.3: Schematic of spin lock. The longitudinal magnetization (black arrow) is rotated into the transverse plane by a $\pi/2$ pulse about the y-axis. A strong RF field (red arrow) is applied along the x-axis which causes the magnetization to precess about the spin lock axis.

Under free precession about z-axis for time τ , the basis vectors evolve under a chemical shift Ω as:

$$I_x \rightarrow I_x \cos(\Omega\tau) + I_y \sin(\Omega\tau) \quad (2.11)$$

$$I_y \rightarrow I_y \cos(\Omega\tau) - I_x \sin(\Omega\tau) \quad (2.12)$$

$$I_z \rightarrow I_z \quad (2.13)$$

If we set the RF frequency offset at $\nu_{avg} = \frac{\nu_I + \nu_S}{2}$, the chemical shifts will be $\pm\Delta\nu/2$ where $\Delta\nu = \nu_I - \nu_S$ which is equal to 105 Hz for 2,3,6-trichlorophenol in a 500 MHz Bruker NMR spectrometer.

In order to prepare LLC of the two proton nuclei, we first apply a $\pi/2$ pulse along the x-axis. Then, we let the system evolve under the chemical shift for a time $\tau = \frac{1}{2\Delta\nu}$ so that the system reaches the state $I_x^I - I_x^S$ and then apply the spin lock along the x-axis to change to the singlet triplet basis, thus creating LLC. The pulse sequence used to prepare the LLC is shown in Fig. 2.4. The corresponding change of state is:

$$I_z^I + I_z^S \xrightarrow{(\pi/2)_x} -I_y^I - I_y^S \xrightarrow{\tau = \frac{1}{2\Delta\nu}} I_x^I - I_x^S \xrightarrow{SpinLock} |S_0\rangle \langle T_0| + |T_0\rangle \langle S_0| \quad (2.14)$$

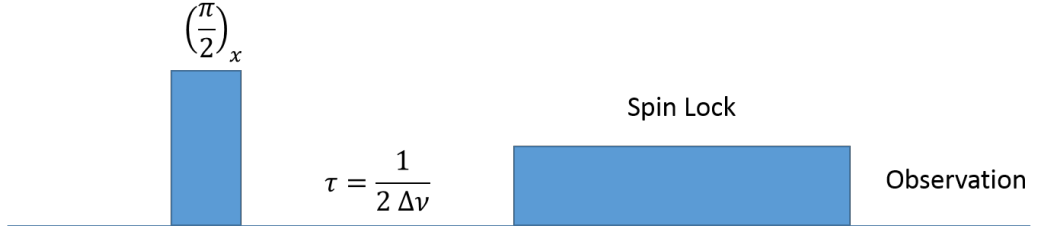


Figure 2.4: Schematic of LLC preparation

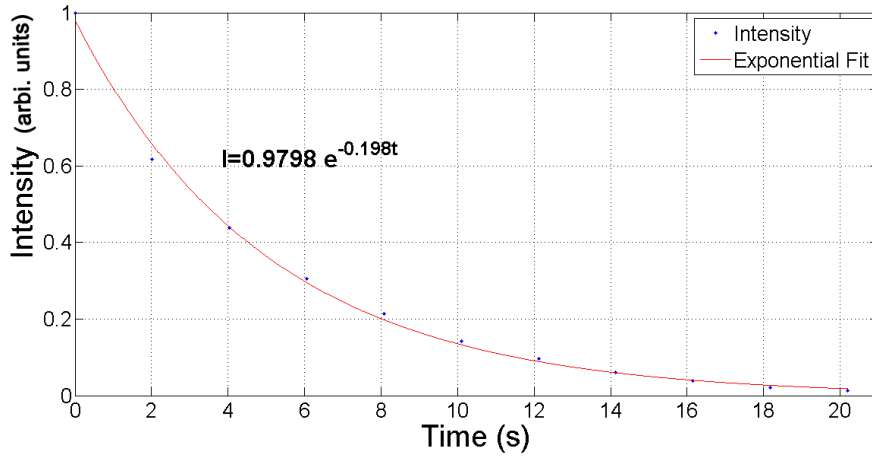


Figure 2.5: An exponential fit to the decaying signal of LLC under a CPMG sequence with the delay between π pulses $\tau = 2.02s$

2.2.2 Measuring Noise Spectrum

By varying the duration 2τ between π pulses, we scan over the corresponding range of frequencies ω . For each ω , we measure the T_2 or dephasing time of the qubit. This is done flipping the magnetization to the transverse plane and monitoring the intensity of the signal obtained over the duration of the CPMG sequence. In order to avoid phase modulation due to J-evolution, we choose the time points (t_i) of our measurement such that $\frac{t_i}{1/J} = integer$. We fit an exponential to the decay of intensity and calculate the T_2 value as the inverse of the decay constant. A representative fit is shown in Fig. 2.5.

Once the LLC is prepared, we measure the noise spectrum by the method described in Sec. 2.1, the only difference being that in place of the delay time τ , we have the spin lock. The method is shown pictorially in Fig. 2.6. A point to be noted is that one should ensure that the phase of the spin lock and π pulses should coincide with that of the coherence to be preserved e.g.

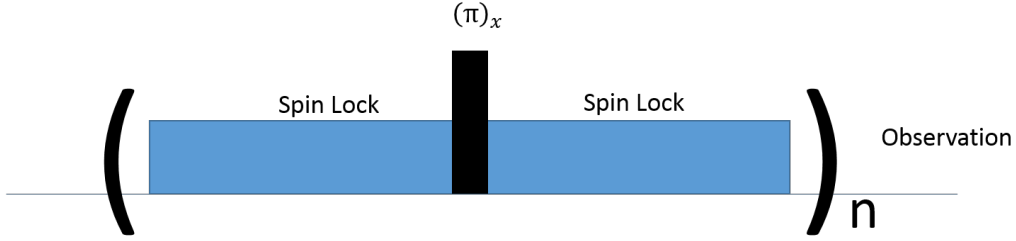


Figure 2.6: Schematic of LLC preparation. For different spin lock durations between the π pulses, we measure the T_2 value of LLC from which the noise spectrum is calculated

spin lock and π pulses should be about x-axis if we wish to prepare LLC from $I_x^1 - I_x^2$ and along y-axis if we are doing the reference state $I_y^1 - I_y^2$.

We measure the noise spectrum of LLC in three fields- 400 MHz, 500 MHz and 600 MHz- and compare it to $-I_y^I - I_y^S$ which corresponds to the state $\frac{i}{\sqrt{2}}(|T_0\rangle\langle T_+| - |T_0\rangle\langle T_-| - |T_+\rangle\langle T_0| + |T_-\rangle\langle T_0|)$ under spin lock. This state is outside the decoherence free subspace and helps us to quantify and compare the performance of the protection offered by the decoherence free subspace. We do this comparison at three different magnetic field strengths, since under strong fields, we expect LLC lifetime to be less as a stronger field's symmetry breaking strength being more, it will be more difficult to nullify its effect using a spin lock. Hence, under the same spin lock strength, we would expect LLCs to have shorter lifetimes in stronger fields.

2.3 Results

The noise spectral densities at different fields (400 MHz, 500 MHz and 600 MHz) are shown in Figs. 2.7, 2.8 and 2.9. We can clearly see that the noise in the decoherence free subspace i.e. the long lived coherence (LLC) given by,

$$\rho_{LLC} = |S_0\rangle\langle T_0| + |T_0\rangle\langle S_0|$$

is much less than that of the unprotected state, which are states that do not belong to the decoherence free subspace. They are given by,

$$\rho_{unprotected} = \frac{i}{\sqrt{2}}(|T_0\rangle\langle T_+| - |T_0\rangle\langle T_-| - |T_+\rangle\langle T_0| + |T_-\rangle\langle T_0|)$$

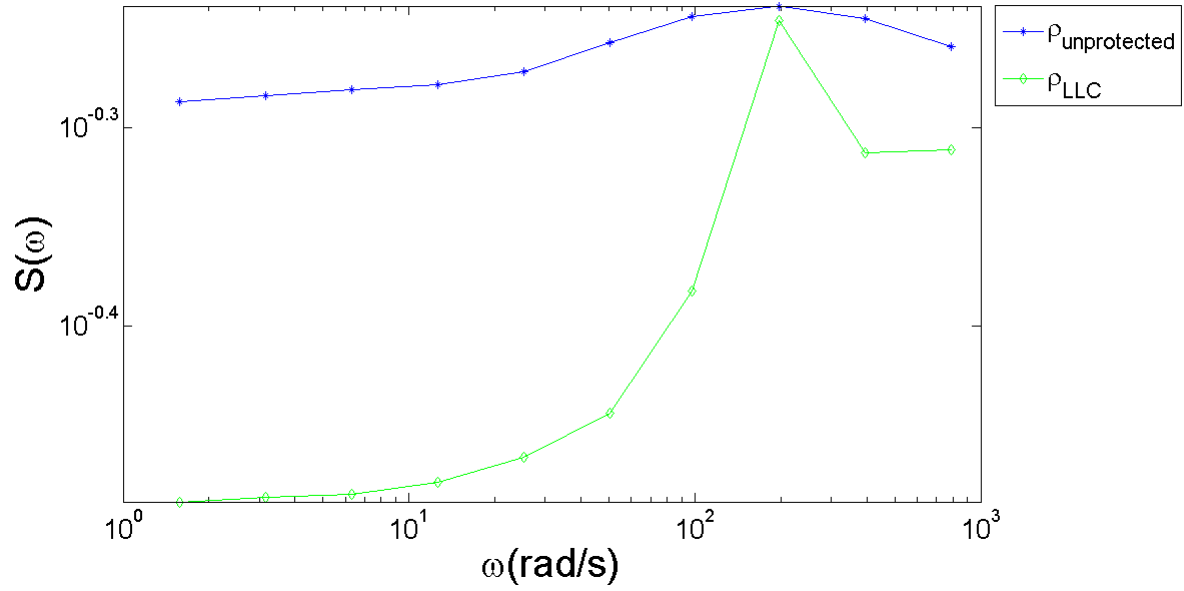


Figure 2.7: Noise spectral density profile of LLC and the unprotected state at 400 MHz field

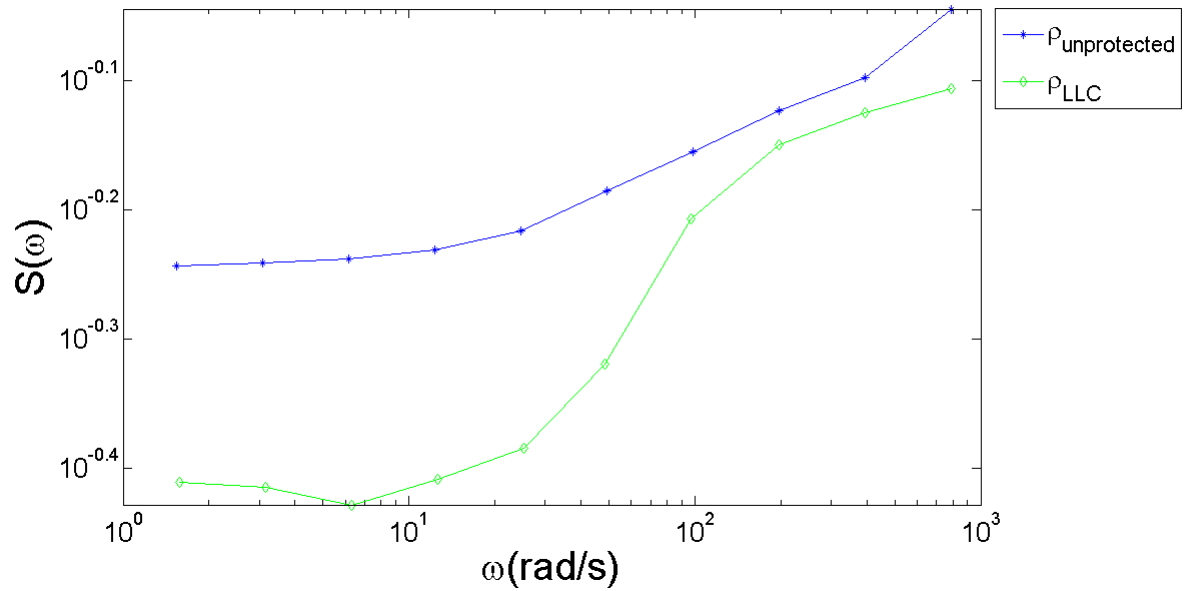


Figure 2.8: Noise spectral density profile of LLC and the unprotected state at 500 MHz field

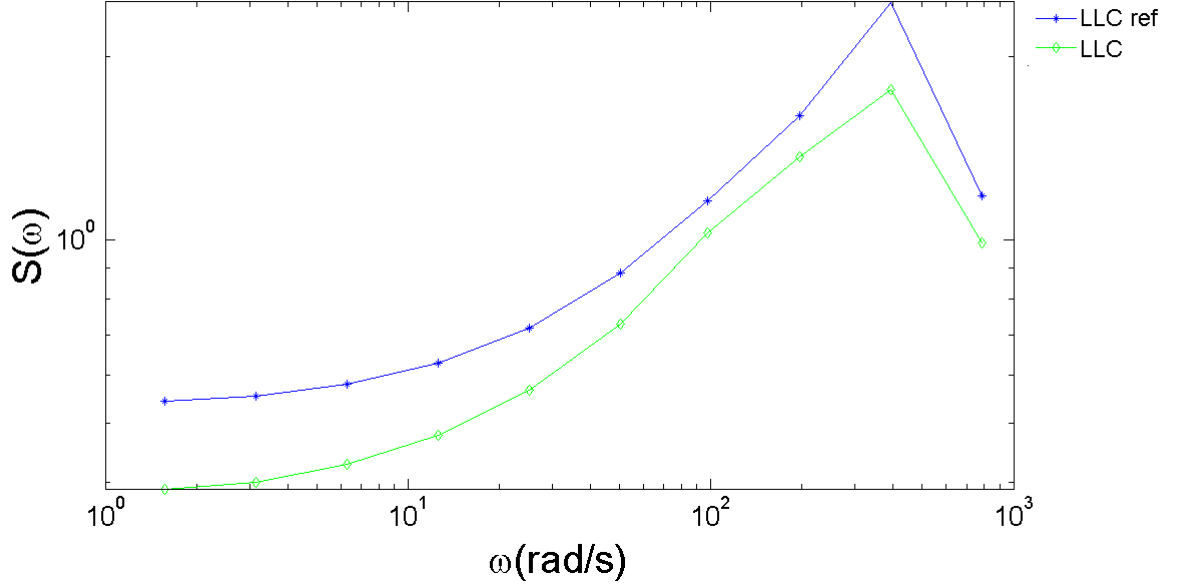


Figure 2.9: Noise spectral density profile of LLC and the unprotected state at 600 MHz field

| ω (rad/s) | T_2 (LLC)(s) | T_2 (unprotected)(s) | ω (rad/s) | T_2 (LLC)(s) | T_2 (unprotected)(s) | ω (rad/s) | T_2 (LLC)(s) | T_2 (unprotected)(s) |
|------------------|----------------|------------------------|------------------|----------------|------------------------|------------------|----------------|------------------------|
| 785.40 | 2.49 | 2.09 | 785.40 | 3.15 | 2.74 | 785.40 | 5.05 | 4.48 |
| 394.18 | 1.40 | 1.00 | 392.70 | 3.29 | 3.09 | 394.18 | 5.07 | 4.33 |
| 196.45 | 1.80 | 1.54 | 196.35 | 3.49 | 3.28 | 196.45 | 4.34 | 4.27 |
| 97.56 | 2.40 | 2.12 | 97.26 | 3.98 | 3.53 | 97.56 | 5.96 | 4.33 |
| 50.30 | 3.39 | 2.79 | 48.63 | 5.15 | 3.79 | 50.30 | 6.86 | 4.46 |
| 25.14 | 4.35 | 3.44 | 25.13 | 5.98 | 4.06 | 25.14 | 7.23 | 4.61 |
| 12.57 | 5.16 | 3.93 | 12.57 | 6.33 | 4.20 | 12.57 | 7.44 | 4.68 |
| 6.28 | 5.75 | 4.25 | 6.28 | 6.62 | 4.27 | 6.28 | 7.55 | 4.71 |
| 3.14 | 6.15 | 4.44 | 3.14 | 6.42 | 4.30 | 3.14 | 7.57 | 4.74 |
| 1.57 | 6.31 | 4.53 | 1.57 | 6.36 | 4.33 | 1.57 | 7.61 | 4.77 |

(a) At 600 MHz

(b) At 500 MHz

(c) At 400 MHz

Figure 2.10: T_2 values (in seconds) at different CPMG frequencies ω for each field. ω is shown in units of rad/s.

2.4 Conclusion and Discussion

Although theoretical calculations clearly indicate that logical qubits encoded in decoherence free subspaces are better protected against noise than unencoded qubits, as far as we are aware, a measurement of the degree of protection offered by decoherence free subspaces has not been made via noise

spectroscopy before. We quantified and characterized this protection by measuring the spectral distribution of noise in the decoherence free subspace in NMR systems. By measuring the noise spectrum of states within and outside the DFS under three different magnetic field strengths (400 MHz, 500 MHz, 600 MHz), we confirm and quantify the protection offered by the DFS. Encoding in the DFS increases the lifetime (T_2) of the quantum state by as much as 2.84 s in 400 MHz field, 2.34 s in 500 MHz field and 1.8 s in 600 MHz field. In the noise spectrum, we also observe that there is a peak in the noise amplitude at around 394 Hz. We conclude by reiterating that the measurement of spectral distribution of noise over a frequency range will enable us to improve existing dynamical decoupling sequences, forming the platform for more efficient decoherence suppression methods.

Chapter 3

Frustrated Decoherence

This chapter is based on the paper <http://arxiv.org/abs/1602.03026> by the author.

In this chapter, two models of decoherence engineering, one proposed by Teklemariam *et al* [11] and the other by Kondo *et al* [17], are presented. We also introduce a model for amplitude damping from our previous work. In both models of decoherence viz. dephasing and spin flip models, we combine the two methods of engineering decoherence in finite dimensional systems, namely the stochastic kick method and the temporally randomized π pulse method. We report the *suppression* of decoherence in the presence of two noise sources at certain resonant conditions, analogous to the frustration of spins in condensed matter systems -hence termed *frustrated decoherence*. We also note that the use of two noise sources can preserve the coherence better than dynamical decoupling sequences at low frequencies. The studies in this chapter are numerical and are likely to be explored experimentally in the future.

3.1 Engineered Decoherence

3.1.1 Stochastic Kick Method

Zurek considered n two level systems interacting via the zz interaction in order to model dephasing [18]. If we take $n = 1$ as the system of interest and consider the interaction between this qubit and the remaining two level systems, the combined two level system will have the Hamiltonian

$$H_{int} = \sum_{k=2}^n J_{1k} \sigma_z^1 \sigma_z^k. \quad (3.1)$$

where J_{1j} are the coupling constants. The evolved system-environment density matrix for a time t is

$$\rho^{SE}(t) = e^{-iH_{int}t} \rho^{SE}(0) e^{-iH_{int}t}$$

Now, we trace out the environmental degrees of freedom to obtain the system density matrix.

$$\rho^S(t) = Tr_E\{\rho^{SE}(t)\}$$

$$\rho^S(t) = \begin{pmatrix} \rho_{00}^S(t) & \rho_{01}^S(t) \\ \rho_{10}^S(t) & \rho_{11}^S(t) \end{pmatrix}.$$

The diagonal terms, ρ_{00} and ρ_{11} , remain unchanged under zz interaction (since the total Hamiltonian commutes with σ_z , the states $|0\rangle_S$ and $|1\rangle_S$, being eigenstates, do not evolve) while the off diagonals, which characterize the system coherence, evolve. Assuming the initial environmental qubits to be in an arbitrary states $|\phi\rangle_k = \alpha_k |0\rangle_k + \beta_k |1\rangle_k$ and the system to be in the initial pure state $|\psi\rangle = a |0\rangle + b |1\rangle$, the system coherence at time t is calculated as

$$\rho_{01}^S(t) = \langle 0 | \rho^S(t) | 1 \rangle$$

$$\rho_{01}^S(t) = ab * z(t)$$

with

$$z(t) = \prod_{k=2}^n |\alpha_k|^2 \exp(-2iJ_{1k}t) + |\beta_k|^2 \exp(2iJ_{1k}t). \quad (3.2)$$

It has been shown [18] that $z(t)$ will return arbitrarily close to its initial value unless $n \rightarrow \infty$, an unfeasible situation in physical realizations.

Cory's group proposed a simple, solvable model [11] composed of one environmental qubit (E) and one system qubit(S).

$$H_0 = \pi(\nu_S \sigma_z^S + \nu_E \sigma_z^E + \frac{\Omega}{2} \sigma_z^S \sigma_z^E) \quad (3.3)$$

where ν_S and ν_E are chemical shifts and $\frac{\Omega}{2}$ is the coupling strength.

In order to compensate for the limited number of environmental qubits, which in turn leads to a quasiperiodicity in the coherence factor, random amplitude kicks are applied to the environmental qubit, which are of the form

$$K_m^E = \exp(-i\epsilon_m \sigma_y^E)$$

where ϵ_m is randomly chosen from the range $(-\alpha, \alpha)$. For a total evolution time T , these kicks are applied at every T/n intervals. We may define the kick rate as $\Gamma = \frac{n}{T}$. The evolution operator is thus

$$U_{total}(T) = K_n U(T/n) K_{n-1} U(T/n) \dots K_1 U(T/n)$$

where $U(t) = \exp\{-iH_0 t\}$.

The system density matrix at time T is obtained by averaging over all realizations of ϵ_m and tracing out the environmental degrees of freedom

$$\overline{\rho^S(T)} = \int_{-\alpha}^{\alpha} \frac{d\epsilon_m}{2\alpha} \dots \int_{-\alpha}^{\alpha} \frac{d\epsilon_1}{2\alpha} Tr_E \{U_{tot}(T) \rho^{SE}(0) U_{tot}^\dagger(T)\}. \quad (3.4)$$

Now, we consider an initial separable state and expand the system density matrix in the eigenbasis of σ_z ,

$$\rho^{SE}(0) = \left(\sum_{i,j=0,1} \rho_{ij}^S(0) |i\rangle \langle j| \right) \otimes \rho^E(0). \quad (3.5)$$

Next, we convert the evolution operator of $\frac{T}{n}$ seconds under 3.3 and a kick K_1^E to an operator acting only on the environmental qubits by conditionally evaluating them for the two possible states $|0\rangle$ and $|1\rangle$ of the system qubit. Repeating this for the next $n-1$ iterations and averaging, we get

$$\overline{\rho^S(T)} = \sum_{i,j=0,1} \rho_{ij}^S(0) f_{ij}(T, n) |i\rangle \langle j|. \quad (3.6)$$

The factor f_{ij} is calculated as

$$f_{ij}(T, n) = \int_{-\alpha}^{\alpha} \frac{d\epsilon_m}{2\alpha} \dots \int_{-\alpha}^{\alpha} \frac{d\epsilon_1}{2\alpha} Tr_E \{(A_i^E)_n \rho^E(0) (A_j^E)_n\} \quad (3.7)$$

where

$$(A_j^E)_n = K_n^E V_j^E \dots K_2^E V_j^E K_1^E V_j^E. \quad (3.8)$$

The operator V_j^E is obtained after tracing out the system qubit from $U(T/n)$ i.e. $V_j^E = {}_S \langle j| U(T/n) |j\rangle_S$. It is clear that $f_{jj} = 1$. Hence, the final system density matrix is

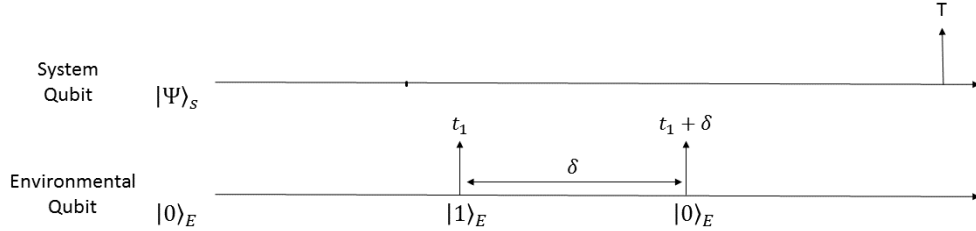
$$\overline{\rho^S(T)} = \begin{pmatrix} \rho_{00}^S(0) & f_{01}(n, T) \rho_{01}^S(0) \\ f_{01}^*(n, T) \rho_{10}^S(0) & \rho_{11}^S(0) \end{pmatrix}.$$

The system coherence is quantified by the off diagonal term $f_{01}(n, T)$, which may be calculated by the repeated application of a superoperator formed from 3.8.

$$\mathcal{O}(\rho) = c(e^{-i\pi(\frac{\Omega}{2} + \nu_E)\sigma_z T/n} \rho e^{-i\pi(\frac{\Omega}{2} - \nu_E)\sigma_z T/n}) \quad (3.9)$$

$$+ d(\sigma_y e^{-i\pi(\frac{\Omega}{2} + \nu_E)\sigma_z T/n} \rho e^{-i\pi(\frac{\Omega}{2} - \nu_E)\sigma_z T/n} \sigma_y) \quad (3.10)$$

Figure 3.1: Schematic representation of Kondo's method: First π pulse is applied at time t_1 and second π pulse at time $t_1 + \delta$



where $c = \frac{1}{2} + \frac{\sin(2\alpha)}{4\alpha}$ and $d = \frac{1}{2} - \frac{\sin(2\alpha)}{4\alpha}$. Using this superoperator, we calculate the system coherence f_{01} as,

$$f_{01}(T, n) = Tr_E[\mathcal{O}^n \rho^E(0)] \quad (3.11)$$

Teklemariam *et al* [11] have analyzed the decoherence factor f_{01} in different regimes of the parameters α and Γ . It has been shown that f_{01} goes to zero for appropriate limits of α and Γ , thus describing phase damping.

3.1.2 Kondo's method

Instead of the random kicks used in the previous method, Kondo *et al* suggested a sequence of temporally randomized π pulses to preempt the use of a large number of environmental qubits [17]. Here also, an interaction of the kind in equation (3.1) is assumed with $n = 2$. We suppose that the initial state of the environmental qubit is $|0\rangle$ and that it is flipped by a π pulse to $|1\rangle$ at a time t_1 . At a time $t_1 + \delta$, it is flipped back into its initial state $|0\rangle$ and we make our observation of the system qubit at a time T . It is schematically shown in figure 3.1. Here, we have two situations

$$H_{int} |\Psi\rangle |0\rangle = J_{12} \sigma_z^S |\Psi\rangle |0\rangle \quad (3.12)$$

$$H_{int} |\Psi\rangle |1\rangle = -J_{12} \sigma_z^S |\Psi\rangle |1\rangle. \quad (3.13)$$

This means that two different operators (3.12) and (3.13) act on the system qubit, conditional on the state of the environmental qubit. To evaluate the state of the system qubit at time T , we apply the unitary

$$e^{-iJ_{12}\sigma_z(T-t_1-\delta)} e^{iJ_{12}\sigma_z\delta} e^{-iJ_{12}\sigma_z t_1} = S(2J_{12}\delta) S(-J_{12}T) \quad (3.14)$$

where $S(\theta) = e^{i\theta\sigma_z}$. Assuming that δ takes on random values from the range $0 \leq 2J_{12}\delta \leq 2\pi$ from time 0 to T, the resultant system density matrix at time T is given by:

$$\overline{\rho^S(T)} = \frac{1}{2\pi} \int_0^{2\pi} d\theta S(\theta) \rho^S(0) S(\theta)^\dagger \quad (3.15)$$

where we have taken $\theta = 2J_{12}\delta$. This simplifies to

$$\overline{\rho^S(T)} = \begin{pmatrix} \rho_{00}^S(0) & \langle e^{i\theta} \rangle \rho_{01}^S(0) \\ \langle e^{-i\theta} \rangle \rho_{10}^S(0) & \rho_{11}^S(0) \end{pmatrix}.$$

For $J_{12}\delta$ uniformly distributed in $[0, 2\pi]$

$$\overline{\rho^S(T)} = \begin{pmatrix} \rho_{00}^S(0) & 0 \\ 0 & \rho_{11}^S(0) \end{pmatrix}. \quad (3.16)$$

which indicates complete dephasing.

3.1.3 Spin Flip Decoherence

In this section, we introduce the xx interaction into Zurek's model [18] and show how this leads to spin flip decoherence. We look at n two level systems with a coupling Hamiltonian of the form

$$H_{SE} = \sum_{k=2}^n J_{1k} \sigma_x^1 \sigma_x^k. \quad (3.17)$$

With the corresponding unitary operator

$$U_{SE}(t) = e^{-iH_{SE}t} = e^{-i \sum_{k=2}^n J_{1k} \sigma_x^1 \sigma_x^k t}. \quad (3.18)$$

Now, we consider a factorisable initial state and express both the system qubit ($k=1$) and the environmental qubits ($k \geq 2$) in the eigenbasis of σ_x . Dropping the subscript $k=1$ for the system qubit,

$$|\Psi(0)\rangle_{SE} = (a' |+\rangle + b' |-\rangle) \otimes \prod_{k=2}^n (\alpha'_k |+\rangle_k + \beta'_k |-\rangle_k). \quad (3.19)$$

The combined state at a time t is given by

$$\begin{aligned}
|\Psi(t)\rangle_{SE} &= U_{SE}(t) |\Psi(0)\rangle_{SE} \\
&= a' |+\rangle \otimes \prod_{k=2}^n e^{-iJ_{1k}\sigma_x t} (\alpha'_k |+\rangle_k + \beta'_k |-\rangle_k) \\
&\quad + b' |-\rangle \otimes \prod_{k=2}^n e^{iJ_{1k}\sigma_x t} (\alpha'_k |+\rangle_k + \beta'_k |-\rangle_k) \\
&= a' |+\rangle \otimes \prod_{k=2}^n e^{-iJ_{1k}t} \alpha'_k |+\rangle_k + e^{iJ_{1k}t} \beta'_k |-\rangle_k \\
&\quad + b' |-\rangle \otimes \prod_{k=2}^n e^{iJ_{1k}t} \alpha'_k |+\rangle_k + e^{-iJ_{1k}t} \beta'_k |-\rangle_k. \tag{3.20}
\end{aligned}$$

Now, we trace out all the environmental qubits in order to get the system density matrix in the $\{|+\rangle, |-\rangle\}$ basis

$$\begin{aligned}
\rho^S(t) &= Tr_E \{ \rho^{SE}(T) \} \\
&= Tr_E \{ |\Psi(t)\rangle_{SESE} \langle \Psi(t)| \}.
\end{aligned}$$

Plugging in equation (3.20) and simplifying using the constraints $\alpha_k'^2 + \beta_k'^2 = 1$ and $a'^2 + b'^2 = 1$, we obtain

$$\begin{aligned}
\rho^S(t)_{\{|+\rangle, |-\rangle\}} &= a'^2 |+\rangle \langle +| + a'b'^* z(t) |+\rangle \langle -| \\
&\quad + a'^* b' z^*(t) |-\rangle \langle +| + b'^2 |-\rangle \langle -| \tag{3.21}
\end{aligned}$$

where $z(t)$ is given by (3.2) with α_k, β_k replaced by their primed versions. This is the density matrix in the $\{|+\rangle, |-\rangle\}$ basis. For converting to the computational basis, we apply the Hadamard transform

$$\rho^S(t)_{\{|0\rangle, |1\rangle\}} = H \rho^S(t)_{\{|+\rangle, |-\rangle\}} H^\dagger \tag{3.22}$$

with

$$H = \frac{1}{\sqrt{2}} \begin{pmatrix} 1 & 1 \\ 1 & -1 \end{pmatrix}.$$

On solving, we get

$$\rho^S(t)_{\{|0\rangle, |1\rangle\}} = \frac{1}{2} \begin{pmatrix} 1 + (\omega + \omega^*) & a'^2 - b'^2 - (\omega - \omega^*) \\ a'^2 - b'^2 + (\omega - \omega^*) & 1 - (\omega + \omega^*) \end{pmatrix}. \tag{3.23}$$

where $\omega = a'b'^* z(t)$. In the limit $n \rightarrow \infty$, we have $\omega \rightarrow 0$.

$$\rho^S(t)_{\{|0\rangle, |1\rangle\}} = \frac{1}{2} \begin{pmatrix} 1 & a'^2 - b'^2 \\ a'^2 - b'^2 & 1 \end{pmatrix}. \tag{3.24}$$

By considering the case $n = 2$, we can clearly see that the term $(\omega + \omega^*)$ causes oscillations in the population levels quantified by the diagonal elements of the density matrix. For large n , we see that the populations of $|0\rangle$ and $|1\rangle$ become equal. It is worth noting that although the physical situations are very different, mathematically, the form of state (3.24) is related by a simple Hadamard transform to the state (3.16).

3.2 Combining the two methods of engineered decoherence

In this section, we describe how the methods of engineering decoherence as mentioned in 3.1.1 and 3.1.2 are combined, in both the phase damping model and spin flip decoherence model. For both interactions, analysis is done for three cases:

1. Under the application of random amplitude kicks
2. Under the application of random kicks and a dynamical decoupling (DD) sequence to suppress decoherence.
3. Under the combined application of random amplitude kicks and a temporally randomized π pulse sequence

3.2.1 Phase damping model

Using the superoperator formalism described in Sec. 3.1.1, we can easily analyze the time evolution of the coherence factor $f_{01}(t)$ for various kick rates in the random amplitude kick model. In order to see the effect of a dynamical decoupling sequence, one only needs to incorporate π pulses after the required number of iterations of the superoperator as determined by the frequency of the decoupling sequence. To see the effect of a temporally randomized π pulse sequence on the environmental qubit, one applies a π pulse about the x-axis to the environmental qubit after a random number of iterations of the superoperator. Here, we generate a random number after each iteration and apply the π pulse if the number is greater than 0.5. The crucial part of the temporally randomized π pulse sequence is the averaging procedure, which is carried out at each point where the coherence factor needs to be calculated.

3.2.2 Spin flip model

As noted before, except for a change of basis, the mathematical formalism for the spin flip model is more or less the same as that of the phase damping model, although we are looking to analyze different quantities viz. the coherence factor in phase damping and the population levels in amplitude damping. The change is that the σ_z operators in the superoperator changes to σ_x operators and we give initial states in the $\{|+\rangle, |-\rangle\}$ basis. To see how the population levels vary over time for different kick rates and how they are affected by dynamical decoupling sequences, we simply utilize the superoperator formalism once more in our simulations. However, while incorporating the temporally randomized π pulse sequence, there is an important distinction. Since a π pulse about the x-axis (σ_x operator) commutes with the noise operator, we apply randomized π pulse about the y-axis (σ_y operator) which does not commute with the noise operator σ_x . All other procedures remain same for calculating the population levels.

3.2.3 Bloch Sphere Distortions

To get a pictorial representation, we can also calculate how the Bloch sphere evolves over time in both phase damping model and the spin flip model. Once we calculate the density matrix at time t , $\rho(t)$, we can calculate the coordinates of the Bloch vector as $n_{x,y,z}(t) = Tr[\sigma_{x,y,z}\rho(t)]$. This way, we can reconstruct the Bloch sphere at any time t .

3.3 Results

3.3.1 Dephasing Model

Although the decoherence rate is enhanced as expected at most kick rates, there is a suppression of decoherence when the kick rate is close to the system-environment coupling, given by $\frac{\Omega}{2}$. Furthermore, it can be shown that this suppression outperforms the dynamical decoupling sequence composed of a series of equidistant π pulses for low frequencies of the decoupling pulses.

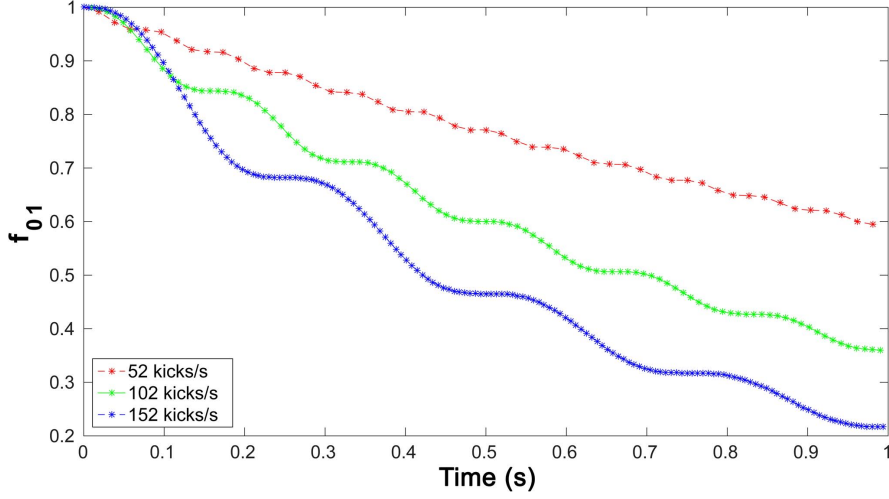


Figure 3.2: Time evolution of decoherence factor f_{01} under different kick rates. Coupling constant $\Omega/2 = 150$ Hz.

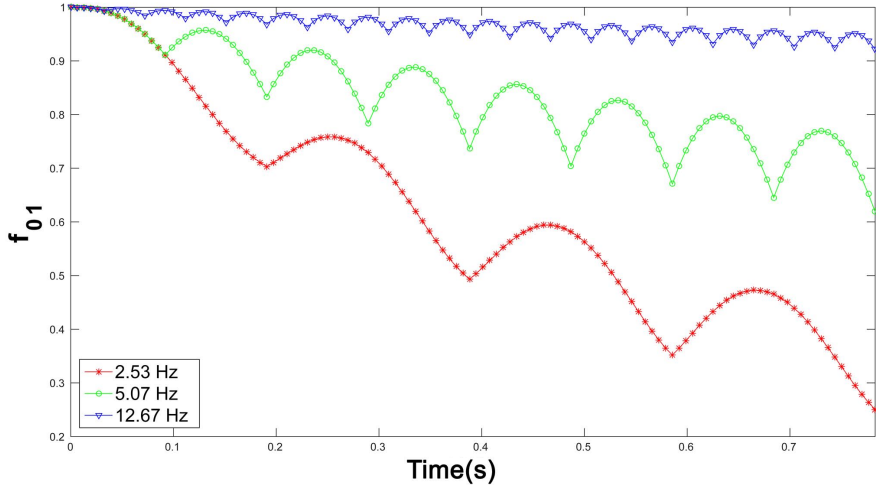


Figure 3.3: Time evolution of decoherence factor f_{01} under different decoupling frequencies. Kick rate is 152 kicks/s, Coupling constant $\Omega/2 = 150$ Hz

For simulations, we assume that the system starts from the initial state $\rho^S(0) = \frac{1}{2}(I + \sigma_x)$ and the environmental qubit is in the thermal equilibrium state $\rho^E(0) = \frac{1}{2}(I + \sigma_z)$. A coupling constant $\Omega/2 = 150$ Hz is assumed. A larger kick rate leads to faster decoherence as shown in Fig. 3.2 . However,

Cory and group have shown that in the limit of very large kick rates, the system gets decoupled from the environment and decoherence is suppressed [11].

On incorporating a randomized π pulse sequence to random amplitude kick model, we observe that the system coherence drops very quickly compared to the decay under random amplitude kicks alone, at most kicks rates as shown in figure 3.4, 3.5. However, when the kick rate is close to the system-environment coupling ($\Omega/2 = 150\text{Hz}$), we observe a suppression of decoherence, as shown in figures 3.6, 3.8 when compared to only applying random amplitude kicks. Furthermore, we see that this suppression due to random π pulses can outperform low frequency dynamical decoupling sequences when the kick rate is close to the resonant frequency of $\Omega/2$. This is shown in figures 3.7, 3.9.

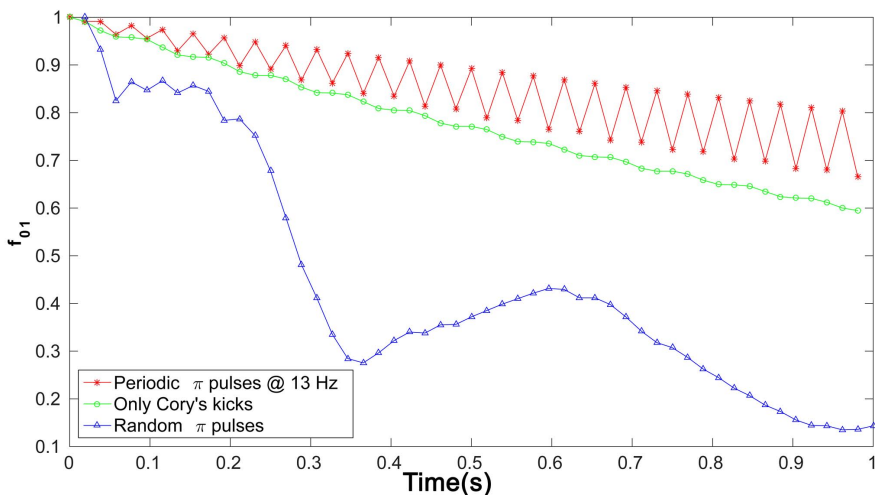


Figure 3.4: Time evolution of decoherence factor f_{01} under a kick rate of 52 kicks/s alone (green), in the presence of kicks and randomized π pulses (blue) and kicks and a DD sequence (red). Coupling constant $\Omega/2 = 150\text{ Hz}$

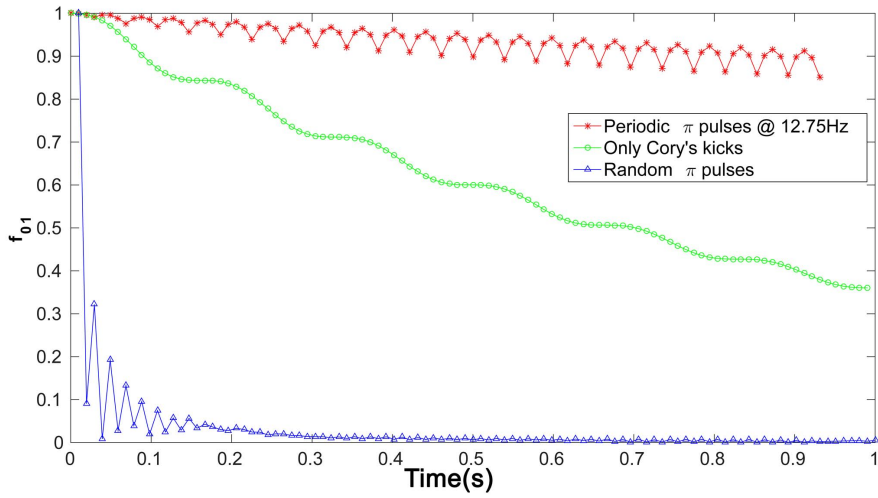


Figure 3.5: Time evolution of decoherence factor f_{01} under a kick rate of 102 kicks/s alone (green), in the presence of kicks and randomized π pulses (blue) and kicks and a DD sequence (red). Coupling constant $\Omega/2 = 150$ Hz

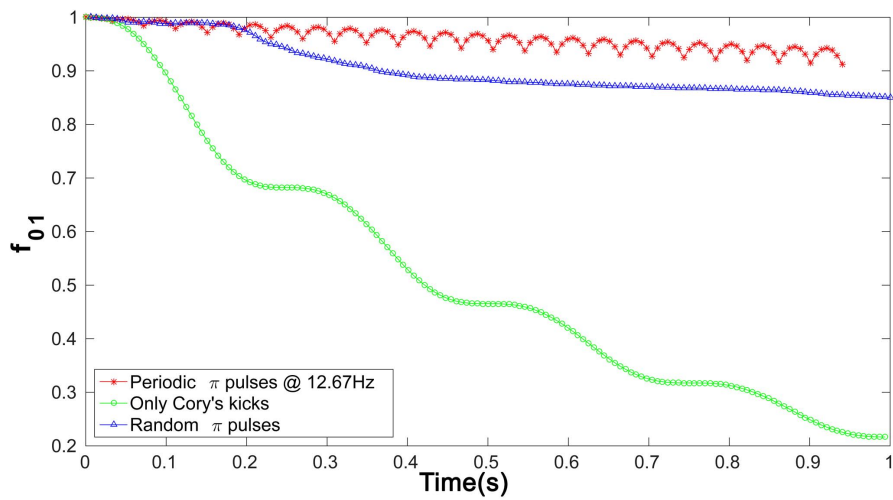


Figure 3.6: Time evolution of decoherence factor f_{01} under a kick rate of 152 kicks/s alone (green), in the presence of kicks and randomized π pulses (blue) and kicks and a DD sequence (red). Coupling constant $\Omega/2 = 150$ Hz

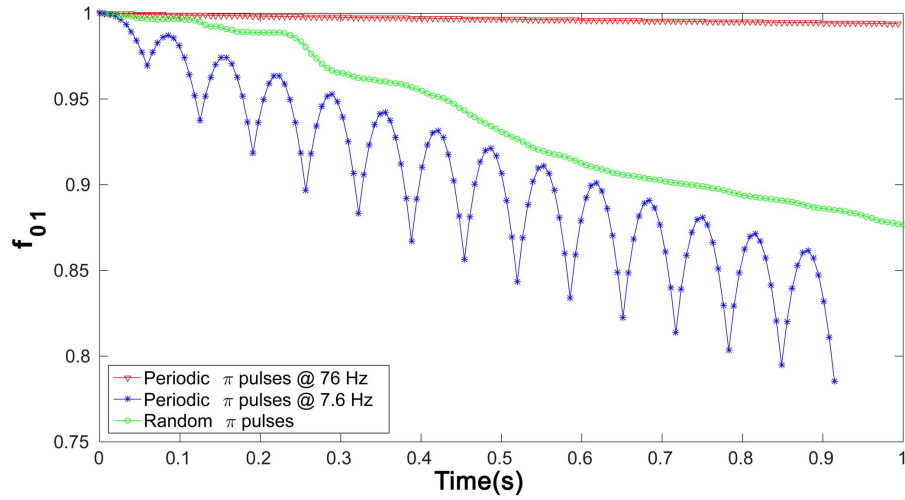


Figure 3.7: Time evolution of decoherence factor f_{01} under a kick rate of 152 kicks/s in the presence of kicks and randomized π pulses (green) and kicks and a DD sequences at 76 Hz (red) and 7.6 Hz (blue). Coupling constant $\Omega/2 = 150$ Hz.

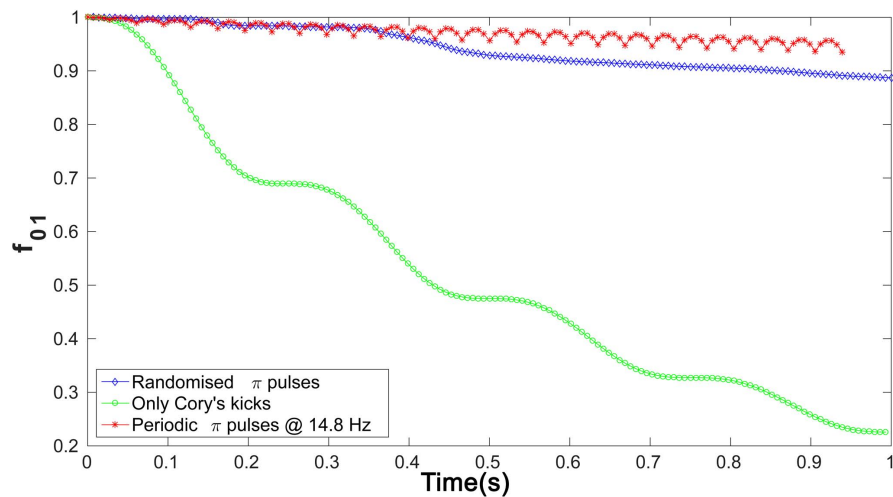


Figure 3.8: Time evolution of decoherence factor f_{01} under a kick rate of 148 kicks/s alone (green), in the presence of kicks and randomized π pulses (blue) and kicks and a DD sequence (red). Coupling constant $\Omega/2 = 150$ Hz.

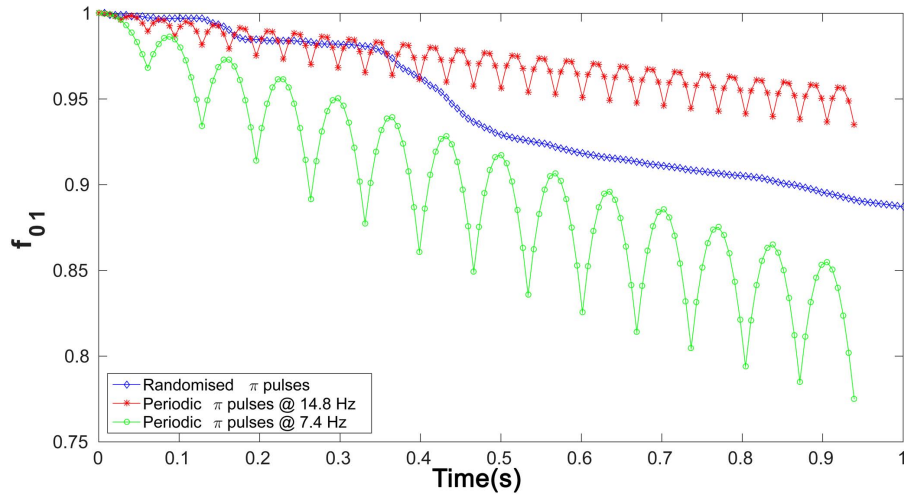


Figure 3.9: Time evolution of decoherence factor f_{01} under a kick rate of 148 kicks/s in the presence of kicks and randomized π pulses (blue) and kicks and a DD sequences at 14.8 Hz (red) and 7.4 Hz (green). Coupling constant $\Omega/2 = 150$ Hz.

Fig. 3.11 gives an integrated picture of how the coherence is affected by coupling strength and kick rates in the presence of temporally randomized π pulses and random amplitude kicks whereas Fig. 3.10 gives the same picture under the influence of random amplitude kicks alone. We observe that at kick rates close to the coupling constant, there is an enhancement in coherence on applying a sequence of π pulses randomized over time.

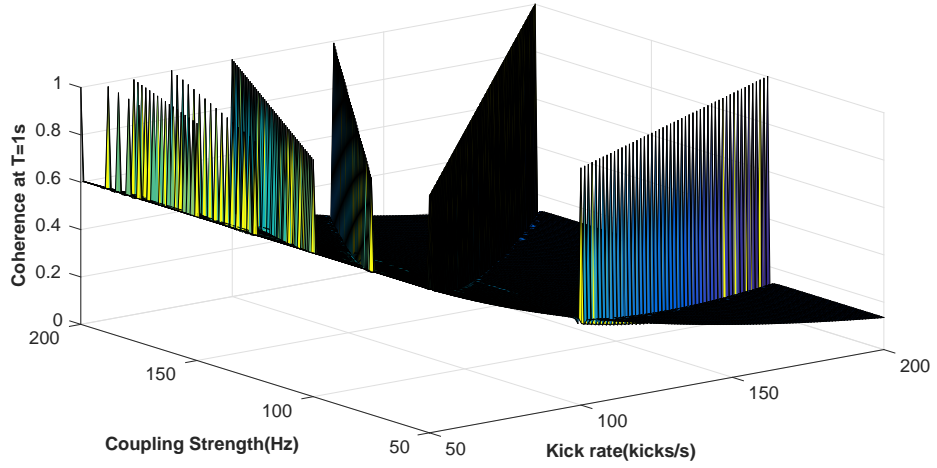


Figure 3.10: Plot of the variation of coherence factor with coupling strength and kick rate at the end of 1s of evolution under the application of random amplitude kicks alone

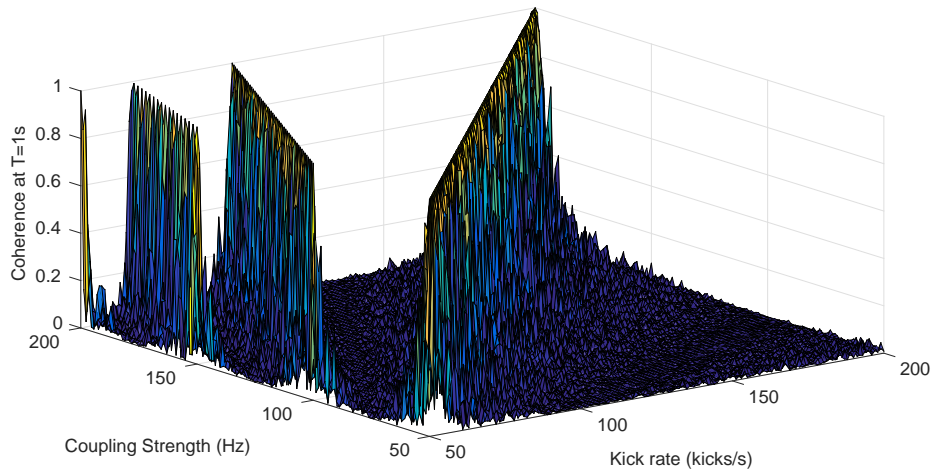


Figure 3.11: Plot of the variation of coherence factor with coupling strength and kick rate at the end of 1s of evolution under the application of random amplitude kicks and randomized π pulses

From Fig. 3.10 it is clear that there is no decoherence when the condition $\frac{\Omega}{2\Gamma} = \text{integer}$ or $\frac{1}{2}\text{integer}$ is satisfied. This can be explained as follows. Each step of evolution under random amplitude kicks is defined by the superoper-

ator 3.10:

$$\mathcal{O}(\rho) = c(e^{-i\pi(\frac{\Omega}{2}+\nu_E)\sigma_z T/n} \rho e^{-i\pi(\frac{\Omega}{2}-\nu_E)\sigma_z T/n}) + d(\sigma_y e^{-i\pi(\frac{\Omega}{2}+\nu_E)\sigma_z T/n} \rho e^{-i\pi(\frac{\Omega}{2}-\nu_E)\sigma_z T/n} \sigma_y) \quad (3.25)$$

We may set $\nu_E = 0$ without loss of generality since while calculating the coherence factor $f_{01}(n, T)$, it comes out as a trivial phase factor. We stress that this does not mean no environmental qubit- it only means that the independent evolution of the environmental qubit has no effect on the system coherence. In other words, here, decoherence is caused due to the *interaction or coupling* with the environmental qubit, which is present even if we set $\nu_E = 0$. Using $n/T = \Gamma$, we write:

$$\mathcal{O}(\rho) = cA + d\sigma_y A \sigma_y \quad (3.26)$$

where,

$$A = [\cos\left(\pi \frac{\Omega}{2\Gamma}\right) I - i\sigma_z \sin\left(\pi \frac{\Omega}{2\Gamma}\right)] \times \rho \times [\cos\left(\pi \frac{\Omega}{2\Gamma}\right) I - i\sigma_z \sin\left(\pi \frac{\Omega}{2\Gamma}\right)].$$

When $\frac{\Omega}{2\Gamma} = m \in \text{Integers}$,

$$A = (-1)^m \rho (-1)^m = (-1)^{2m} \rho = \rho$$

$$\mathcal{O}(\rho) = cA + d\sigma_y A \sigma_y$$

Now, the coherence factor f_{01} is given by

$$f_{01}(n, T) = \text{Tr}_E(\mathcal{O}^n \rho^E(0))$$

After the first iteration in this case,

$$\mathcal{O}(\rho) = c\rho + d\sigma_y \rho \sigma_y \quad (3.27)$$

and,

$$\text{Tr}_E(\mathcal{O}(\rho)) = c\text{Tr}_E(\rho) + d\text{Tr}_E(\sigma_y \rho \sigma_y) \quad (3.28)$$

$$= c\text{Tr}_E(\rho) + d\text{Tr}_E(\rho) \quad (3.29)$$

$$= (c + d)\text{Tr}_E(\rho) \quad (3.30)$$

$$= \text{Tr}_E(\rho) \quad (3.31)$$

where we used the fact that $c + d = 1$. In this case, for n iterations of the superoperator, we will have:

$$\text{Tr}_E(\mathcal{O}^n(\rho)) = \text{Tr}_E(\mathcal{O}^{n-1}(\rho)) \dots = \text{Tr}_E(\mathcal{O}(\rho)) = \text{Tr}_E(\rho). \quad (3.32)$$

This means that the coherence factor remains identical to the initial coherence factor throughout the evolution of the system.

For the case where $\frac{\Omega}{2\Gamma} = (2m + 1)/2, m \in \text{Integers}$,

$$A = -i\sigma_z(-1)^m\rho - i\sigma_z(-1)^m = -\sigma_z\rho\sigma_z$$

Now, the superoperator becomes,

$$\mathcal{O}(\rho) = -c\sigma_z \times \rho \times \sigma_z - d i\sigma_x \times \rho \times -i\sigma_x$$

. And the coherence factor becomes,

$$\text{Tr}_E(\mathcal{O}(\rho)) = -c\text{Tr}_E(\rho) - d\text{Tr}_E(\sigma_x\rho\sigma_x) \quad (3.33)$$

$$= -c\text{Tr}_E(\rho) - d\text{Tr}_E(\rho) \quad (3.34)$$

$$= -(c + d)\text{Tr}_E(\rho) \quad (3.35)$$

$$= -\text{Tr}_E(\rho) \quad (3.36)$$

Hence, after n iterations,

$$\text{Tr}_E(\mathcal{O}^n(\rho)) = (-1)^n\text{Tr}_E(\rho). \quad (3.37)$$

Hence, the absolute value of the coherence factor remains same throughout the evolution of the system.

From Fig. 3.11, we may see that the inclusion of the temporally randomized π pulse sequence drastically increases the decoherence rate at most parameter regimes except when the kick rate is close to or equal to the coupling strength. We also note that the absence of decoherence at $\frac{\Omega}{2\Gamma} = \frac{1}{2}\text{integer}$ values is not observed on including the randomized π pulse sequence. This is because in this case, the coherence flips between -1 and 1 and the averaging procedure wipes out the coherence.

3.3.2 Spin flip Model

For the xx interaction, we work in the $\{|+\rangle, |-\rangle\}$ basis. Hence, we start from the initial state $\rho^S(0)_{\{|+\rangle, |-\rangle\}} = \frac{1}{2}(I + \sigma_x)$ which is equivalent to $\rho^S(0)_{\{|0\rangle, |1\rangle\}} = \frac{1}{2}(I + \sigma_z)$ in the computational basis. The environmental qubit is assumed to be in the thermal equilibrium state $\rho^E(0) = \frac{1}{2}(I + \sigma_z)$. In this case, we monitor the populations of the two states $|0\rangle$ and $|1\rangle$ reflected in the diagonal entries ρ_{00}^S, ρ_{11}^S and look for the oscillations predicted by equation (3.23). We observe that for higher kick rates, the oscillations damp quickly and approach the value 0.5, as predicted. This is illustrated in figure 3.12. Figure 3.13 depicts the sustained oscillations on applying a dynamical decoupling

sequence to the system qubit. We also note that the frequency of oscillation decreases as one approaches the resonant kick rate $\Omega/2$ and then increases again.

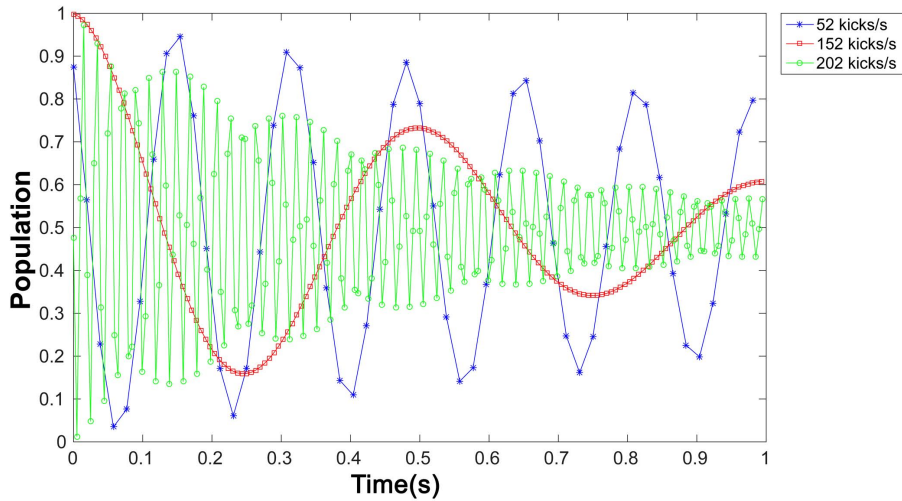


Figure 3.12: Oscillations in population level of state $|0\rangle$ under different kick rates. Coupling constant $\Omega/2 = 150$ Hz

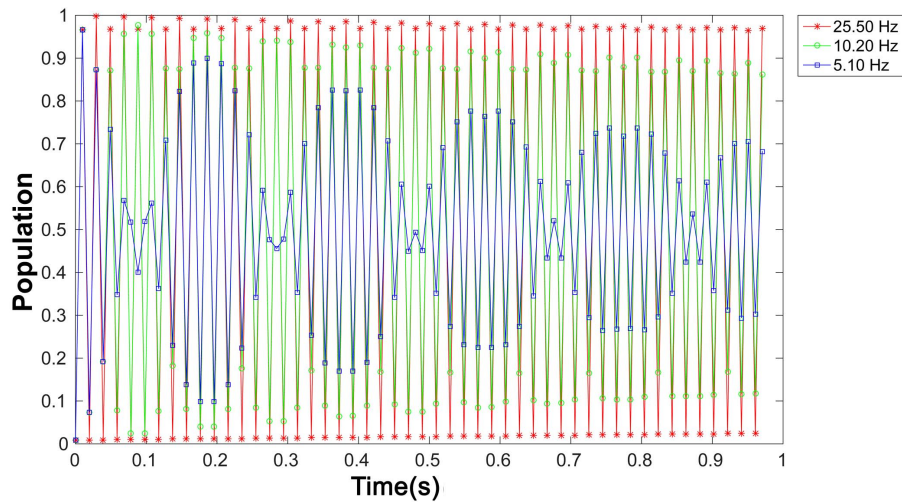


Figure 3.13: Oscillations in population level of state $|0\rangle$ at a kick rate=102 kicks/s with different DD frequencies. Coupling constant $\Omega/2 = 150$ Hz

In this situation, applying a random π pulse sequence causes the oscillations in the system population to damp very quickly to its equilibrium value

$\frac{1}{2}$ (shown in figure 3.14). However, on applying a DD sequence when the kick rate is close to the resonant value, we observe that the system's initial population is conserved, with only a slight leakage over time (figure 3.15). This effect can be explained by considering how the DD sequence works. If the DD sequence is applied at a time t , it attempts to keep the system from evolving from the state in which it existed at time t . Hence, the point of time at which the DD sequence starts is of crucial importance. In other words, the correlation time of the π pulse sequence must be much shorter than the correlation time of the noise to be suppressed. As mentioned before, at the resonant values of the kick rates, the frequency of oscillations decrease. Hence, when the first π pulse of the DD sequence is applied, the system is still not very far away from its initial state. Thus, the DD sequence is able to arrest the evolution of the system very close to its initial state.

Similar to the result obtained on combining random amplitude kicks and temporally randomized π pulses in the phase damping model, we see that when the kick rate is close to the coupling constant between the qubits, damping of the population level oscillations is suppressed. In Fig. 3.15, we see that the suppression offered on combining the two noise sources performs slightly better than a DD sequence.

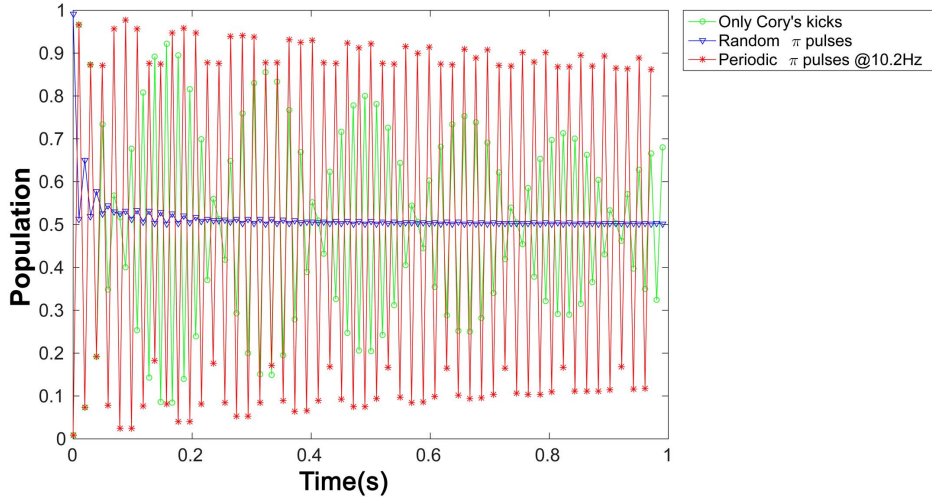


Figure 3.14: Oscillations in population level of state $|0\rangle$ under random amplitude kicks alone (green) - kick rate = 102 kicks/s -, random amplitude kicks and temporally randomized π pulses (blue), and random amplitude kicks and a DD sequence (red). Coupling constant $\Omega/2 = 150$ Hz

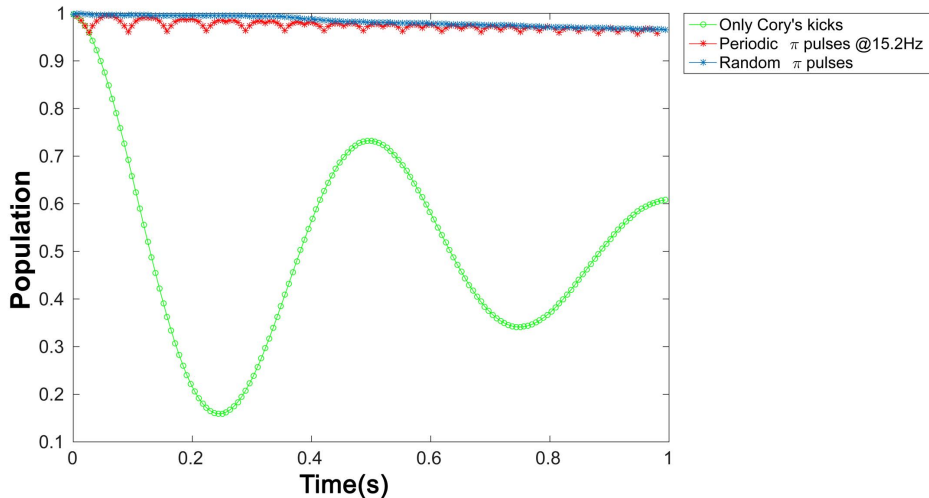


Figure 3.15: Oscillations in population level of state $|0\rangle$ under random amplitude kicks alone (green)-kick rate=152 kicks/s-, random amplitude kicks and temporally randomized π pulses (blue), and random amplitude kicks and a DD sequence (red). Coupling constant $\Omega/2 = 150$ Hz.

3.4 Conclusion and Discussion

As opposed to existing models for phase damping, a model using xx coupling was proposed which can successfully model amplitude damping. This, along with techniques developed by Cory and Kondo, facilitates a controlled study of decoherence using finite resources. It is important to study both kinds of decoherence, phase and amplitude damping, in order to facilitate the development of control strategies to suppress a general decoherence process.

We have also shown that on combining the random kick model and the randomized π pulse sequence method, we obtain faster decoherence rates in the phase damping case. However, when the kick rate is close to the system-environment coupling, it is observed that decoherence is suppressed on applying a temporally randomized π pulse sequence. Viola and Knill [19] have previously identified cases where a random dynamical decoupling sequences can have more relaxed time scale requirements as compared to periodic π pulses and can become superior to existing techniques. Banerjee *et al* [20] have done similar work on the enhancement of geometric phase by frustrated decoherence. In their work, two independent noise baths coupled to the system were considered. A frustration of geometric phase was observed when the coupling strengths to the two baths were equal [20].

The results obtained here demonstrate that a random π pulse sequence to the environmental qubit can help in the preservation of system coherence, sometimes even outperforming a periodic π pulse sequence. In the case of xx interaction, the combination of the two randomization techniques achieve a faster decoherence rate, but exhibit suppressed decoherence when the kick rate is close to the coupling constant between the two qubits. Furthermore, due to decreased oscillation frequency when the kick rate is close to the coupling to the environment, dynamical decoupling proves to be very effective at this kick rate.

Chapter 4

Quantum Control in Equivalent Spins

In this chapter, we first introduce the notion of qubits, the Bloch sphere representation and the group theoretic formulation of quantum control. We then describe the use of actuator qubits for quantum control in the context of decoherence free subspaces. Theoretically, the possible quantum mechanical operations on a quantum system can be understood and calculated in terms of the dynamical Lie algebra of the system and control Hamiltonians. This is also described in this chapter. Finally, the experimental method used to realize universal quantum control, which enables improved decoherence free subspaces, and the corresponding results are presented.

4.1 Qubits and the Bloch Sphere

A qubit is the quantum analogue of a classical bit. In theory, any two level quantum system may be considered as a qubit. Many systems have been adopted as qubits-such as electronic spins in diamonds, nuclear spins, photons, spins in quantum dots and trapped ions. The crucial difference between a bit and a qubit is that while a bit can only exist in one of the possible states 0 or 1, the qubit, being a quantum mechanical object, may exist in an arbitrary superposition of 0 and 1 which allows one to utilize quantum phenomena.

$$|Qubit\rangle = \frac{\alpha |0\rangle + \beta |1\rangle}{\sqrt{2}}$$

where $|\alpha|^2 + |\beta|^2 = 1$. Without loss of generality, we may obtain a pictorial representation of a qubit by putting $\alpha = \cos(\frac{\theta}{2})$ and $\beta = e^{i\phi} \sin(\frac{\theta}{2})$. This

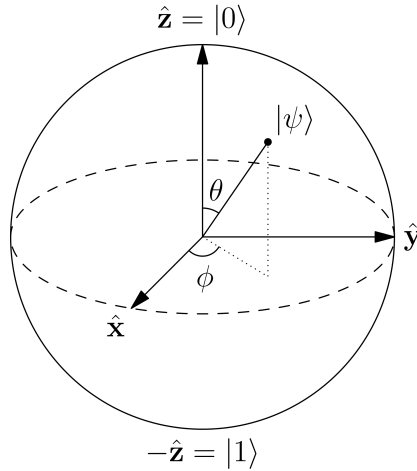


Figure 4.1: Bloch sphere representation of an arbitrary qubit state $|\Psi\rangle = \cos(\frac{\theta}{2})|0\rangle + e^{i\phi}\sin(\frac{\theta}{2})|1\rangle$. Image by Glosser.ca, Wikimedia Commons

yields the representation of a unit sphere with $0 \leq \theta \leq \pi$ and $0 \leq \phi \leq 2\pi$ as denoted in the figure 4.1

4.2 Quantum Control

In this section, we briefly review the definition of Lie algebras before describing how it relates to quantum control. Simply put, we say that we have universal control over a qubit when we can rotate it to anywhere on the Bloch sphere through one or more operations. The use of Lie algebra formalism will help us to formally calculate the set of control operations possible on the qubit, given the internal and control Hamiltonians.

4.2.1 Lie Algebras and Lie Groups

We define a Lie algebra as follows[21]:

Definition 4.2.1. A vector space over a field \mathcal{F} , along with an added binary operation called the Lie bracket $[\cdot, \cdot] : \mathcal{L} \times \mathcal{L} \rightarrow \mathcal{L}$, is called a Lie algebra \mathcal{L} . For every ordered pair of elements $\{x, y\}$, the Lie bracket associates an element $[x, y]$ in \mathcal{L} . The Lie bracket satisfies the following axioms:

1. Bilinearity: For all $x, y, z \in \mathcal{L}$ and $\alpha, \beta \in \mathcal{F}$

$$[\alpha x + \beta y, z] = \alpha[x, z] + \beta[y, z],$$

$$[x, \alpha y + \beta z] = \alpha[x, y] + \beta[x, z],$$

2. Alternativity:

$$[x, x] = 0 \forall x \in \mathcal{L}$$

3. Jacobi identity: For all $x, y, z \in \mathcal{L}$

$$[x, [y, z]] + [y, [z, x]] + [z, [x, y]] = 0$$

For a Lie group, we use the following definition[21]:

Definition 4.2.2. A Lie group is a kind of group which is also an analytic, differential manifold where the operations of multiplication $\{x, y\} \rightarrow xy$ and inversion $x \rightarrow x^{-1}$ are analytic

4.2.2 Controllability

Consider the Schrödinger equation,

$$i\hbar \frac{\partial \psi}{\partial t} = \mathcal{H}(g)\psi \quad (4.1)$$

where g belongs to a space of functions \mathcal{G} . The set of possible control operations on the state ψ are unitary matrices of the form $e^{-\frac{i}{\hbar} \int \mathcal{H}(g) dt}$. Formally, we may define them as given below[21]:

Definition 4.2.3. The set of possible control operations U on a state obeying Eqn. 4.1 is the connected Lie group corresponding to the Lie algebra \mathcal{L} , generated by the span of $-\frac{i}{\hbar} \mathcal{H}(g), g \in \mathcal{G}$.

The Lie algebra thus generated is called the dynamical Lie algebra of the system. In general, for an n dimensional state vector, the dynamical Lie algebra will always be a subalgebra of $u(n)$, the Lie algebra of $n \times n$ skew-Hermitian matrices. We have complete control over the system when $\dim(\mathcal{L}) = \dim(u(n))$, which is equal to n^2 . Correspondingly, the Lie group $e^{\mathcal{L}} = U(n)$, the set of all unitary matrices in n dimensions. This means that with the suitable choice of control parameters $g \in \mathcal{G}$, one may obtain any $n \times n$ unitary matrix.

4.2.3 Basis of a dynamical Lie Algebra

Given a set of vectors $\{v_1, v_2, v_3 \dots v_n\}$ in a Lie algebra \mathcal{L} , a repeated Lie bracket of these elements will yield another element of \mathcal{L} . By repeatedly calculating the Lie bracket until no new linearly independent vector is produced or until the dimension of the Lie algebra becomes equal to n^2 or $n^2 - 1$, one may obtain the dynamical Lie algebra.

4.2.4 Quantum Control in Decoherence Free Subspaces

Although theoretical work [22, 23] indicate that fault tolerant universal quantum control is possible in decoherence free subspaces (DFS), Cappellaro et al [13] have shown that leakage from DFS during state manipulation using radiofrequency pulses in nuclear magnetic resonance (NMR) implementation of qubits is an effectively inevitable problem. Specifically, they have shown that in a DFS encoding of two physical qubits protected against collective dephasing, the use of RF fields necessarily cause the state to go out of the protected subsystem into other parts of the larger Hilbert space where it is subject to decoherence.

A plot of the function,

$$p(t) = \frac{\text{Tr}[(P_L \rho(t))^2]}{\text{Tr}[\rho(t)^2]}$$

where P_L is the projection operator onto the DFS against time clearly illustrates this point. Assuming an initial state $\sigma_z^L = \frac{1}{2}(\sigma_z^1 - \sigma_z^2)$ within the DFS, the evolution of the density matrix under the application of a logical π pulse, equivalent to a π pulse to both the physical qubits,

$$P_x(\pi) = e^{-i\frac{\pi}{2}(\sigma_x^1 + \sigma_x^2)}$$

is considered. The density matrix at time t is given by

$$\rho(t) = e^{-i\omega_{rf}(\sigma_x^1 + \sigma_x^2)t} \sigma_z^L e^{i\omega_{rf}(\sigma_x^1 + \sigma_x^2)t}$$

where ω_{rf} is the RF frequency. $\Delta\omega$ denotes the chemical shift between the two physical spins comprising the logical qubit. It is observed that a full return to the DFS occurs only in the case where $\Delta\omega = 0$, which means that the two spins should be chemically equivalent i.e. have the same precession frequency under the applied magnetic field. However, on making the two spins equivalent, one will lose the ability to selectively control the two spins, which means that universal control of the logical qubit will be lost.

4.2.5 Actuator Based Quantum Control

Although direct control of qubits is possible in many situations, attempts to protect the qubit from noise as well as intrinsically weak interactions with control fields often makes this a difficult task. For example, the interaction strength of nuclear spins is several orders of magnitude smaller than that of electronic spins, which poses additional difficulties in qubit systems which include both electronic and nuclear spins, such as nitrogen vacancy centers in diamond.

Recent works [24, 25] have demonstrated that it is possible to achieve indirect control via actuator qubits coupled to the qubit which we want to control. It has even been shown that actuator based gate times are faster than direct driving in certain situations [26]. The procedure to calculate the possible control operations is as given in Section 4.2.3. We write the total Hamiltonian as:

$$\mathcal{H} = \mathcal{H}_A + \mathcal{H}_T + \mathcal{H}_{AT}$$

where \mathcal{H}_A is the internal Hamiltonian of the actuators, \mathcal{H}_T is the internal Hamiltonian of the targets \mathcal{H}_{AT} is the actuator-target coupling Hamiltonian. Given a control Hamiltonian which acts only on the actuator qubits \mathcal{H}_C , the possible actuator based control operations can be calculated by repeatedly evaluating the commutators between the control Hamiltonian \mathcal{H}_C and the drift Hamiltonian \mathcal{H} [25].

4.3 Experimental Implementation

The spin system chosen in for experiments on universal control was fumaric acid 4.2. In fumaric acid, we see that two protons are chemically equivalent. Hence we do not have the ability to selectively control these spins by direct control. In order to get a third spin to be used as an actuator, we utilize the naturally available ^{13}C atoms present in the sample. Since the relative abundance of ^{13}C is only 1.1%, we take a high concentration of fumaric acid so that the signal from fumaric acid molecules having ^{13}C are strong enough to be detected. Here, we took 25mg of fumaric acid in 600 μ L of deuterated methanol (CD_3OD). Apart from permitting the use of deuterium field lock, the use of a deuterated solvent also replaces the protons attached to the oxygen atoms with deuterium, hence removing unwanted signals from the protons attached to the oxygens.

We now have a three qubit system-two protons which are the target qubits and one ^{13}C molecule which is the actuator qubit. Although the presence of the ^{13}C breaks the chemical equivalence between the two protons in theory,

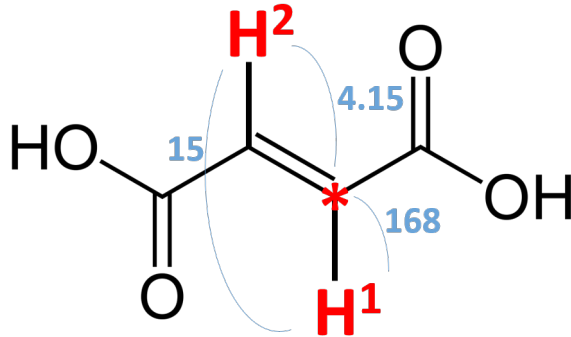


Figure 4.2: Structure of fumaric acid. The red Hs, labelled 1 and 2, are the target nuclear spins. The red star indicates one possible position of the ^{13}C nucleus. Numbers indicate coupling strengths between nuclei in Hz.

the isotopic shift introduced is extremely small ($<1\text{ppm}$). Hence, the system has two *effectively* equivalent protons and one ^{13}C spin. The couplings between these spins are: $J_{H^1H^2} = 15\text{ Hz}$, $J_{^{13}\text{C}H^1} = 168\text{ Hz}$, $J_{^{13}\text{C}H^2} = 4.15\text{ Hz}$. The anisotropy between coupling strengths of ^{13}C and the chemically equivalent protons breaks the *magnetic* equivalence between the two protons. This allows us to indirectly control the two protons independently, even though they are chemically equivalent and cannot be selectively controlled via direct control.

4.3.1 Universal Gates

As NAND and NOR gates are universal in classical logic, for two qubits, a set of universal quantum gates are [27]:

1. Controlled NOT gate: $CNOT = \begin{pmatrix} 1 & 0 & 0 & 0 \\ 0 & 1 & 0 & 0 \\ 0 & 0 & 0 & 1 \\ 0 & 0 & 1 & 0 \end{pmatrix}$

2. Hadamard gate: $H = \frac{1}{\sqrt{2}} \begin{pmatrix} 1 & 1 \\ 1 & -1 \end{pmatrix}$

3. The $\pi/8$ gate: $R(\pi/4) = \begin{pmatrix} 1 & 0 \\ 0 & e^{i\pi/4} \end{pmatrix}$

If we are able to realize these three gates, any other unitary gate operation can be constructed from them. We generated and optimized these gates

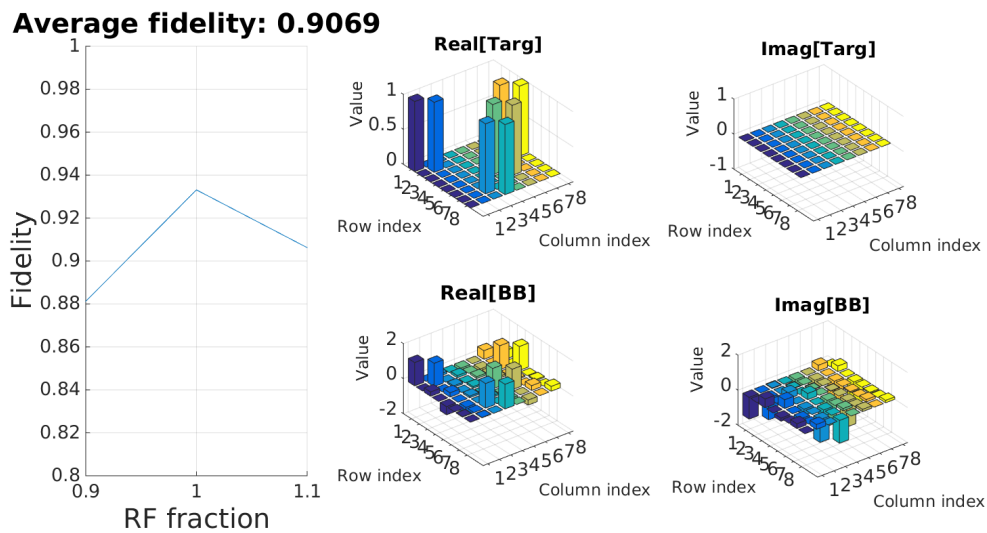


Figure 4.3: Fidelity of the CNOT gate on the two proton nuclei

numerically using the bang-bang control method described by Gaurav *et al* [28] and converted to a pulse program compatible with a Bruker 500 NMR spectrometer in Matlab. The simulated spectra of these three gates are used to compare with and verify the experimental spectra. The fidelities of the three gates and their variation with RF inhomogeneity using this method are as indicated in the Figs. 4.3,4.4 and 4.5.

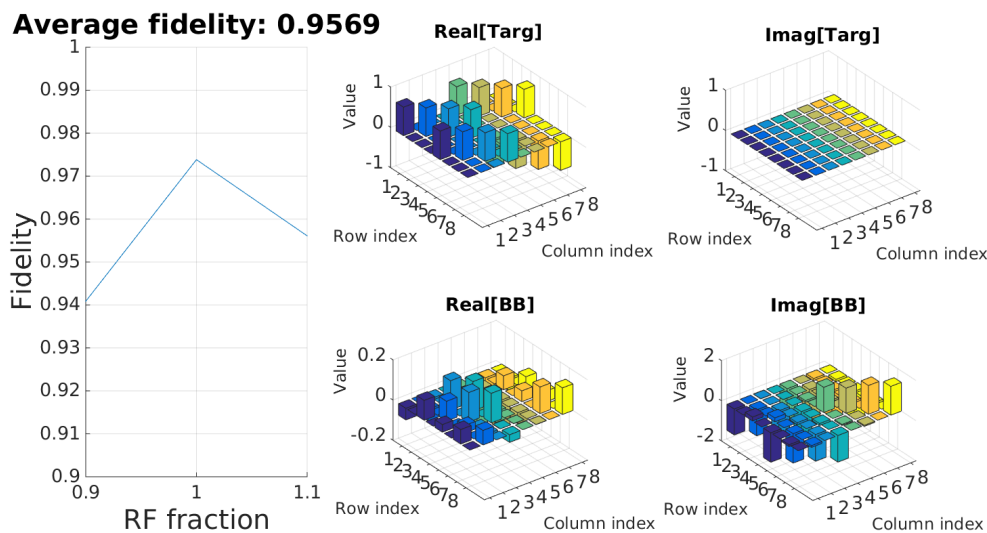


Figure 4.4: Fidelity of the Hadamard gate on the first proton nuclei

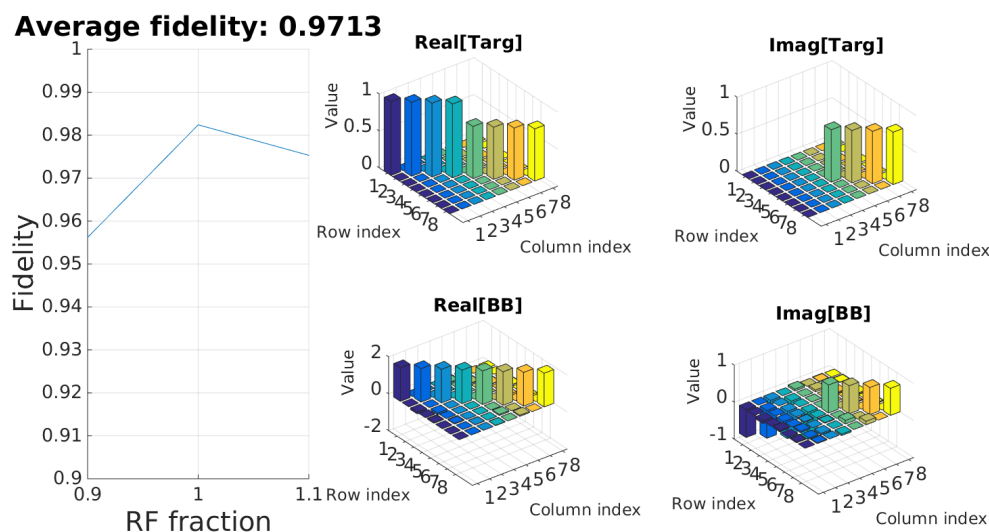


Figure 4.5: Fidelity of the $\pi/8$ gate on the first proton nuclei

4.3.2 Suppressing Superfluous Signals

The bulk of the fumaric acid sample will be composed of molecules which do not have a ^{13}C nucleus in it. Hence, the most intense signal will be a single peak from the equivalent protons, originating from the fumaric acid molecules which do not have a ^{13}C nucleus. However, 1.1% of the molecules will have a ^{13}C nucleus at the position indicated by a star in 4.2. Another 1.1% will have ^{13}C atoms at a symmetrically opposite position, which has an identical spectral signature as the other symmetric molecule. In total, we will get useful signal from only 2.2% of the total sample volume.

While measuring the spectrum of the molecule, we will get signals from both kinds of molecules—those having ^{13}C nuclei and those which do not possess ^{13}C nuclei. Since the high intensity signal from molecules which do not possess ^{13}C nuclei interfere with our experiments, which depend on only the signals from molecules which have ^{13}C nuclei, we initially suppress the proton magnetization by the two methods described below. More importantly, we want to ensure that our gates are acting only on molecules having ^{13}C nuclei and that the resulting spectrum is entirely produced by the action of gates on such molecules. Once the proton magnetization is killed, we regenerate magnetization from ^{13}C nuclei and use it for our experiments.

Magnetic Field Gradients

In many NMR experiments, the magnetic field about which the spins are precessing is deliberately made as homogeneous as possible. Ideally, one

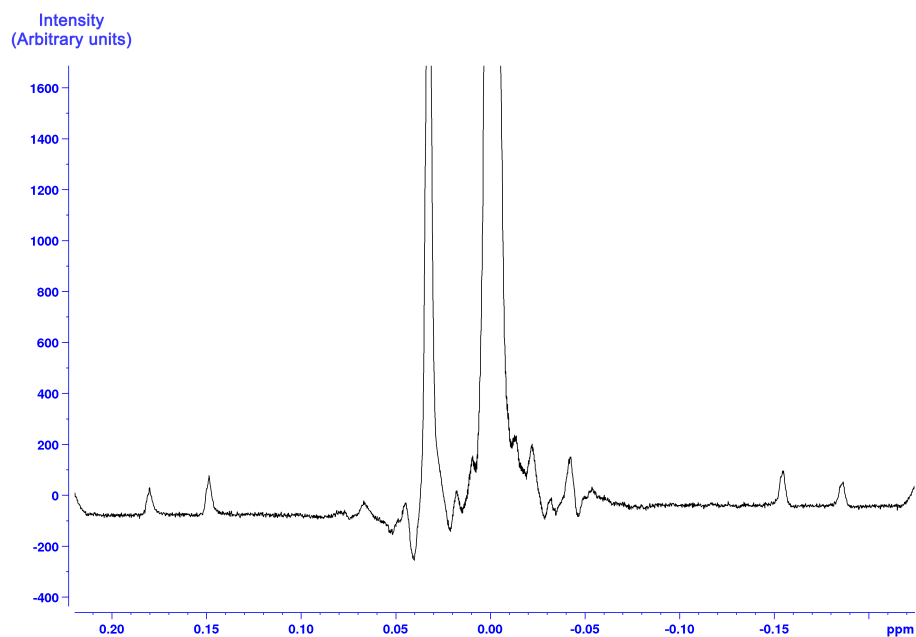


Figure 4.6: Spectrum of fumaric acid without suppression

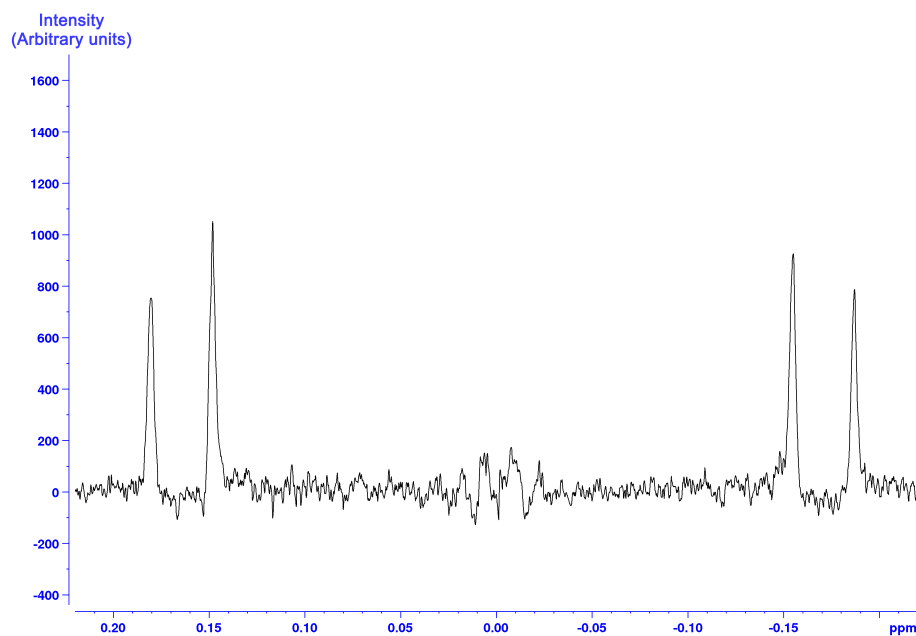


Figure 4.7: Spectrum of fumaric acid after suppression of central peak

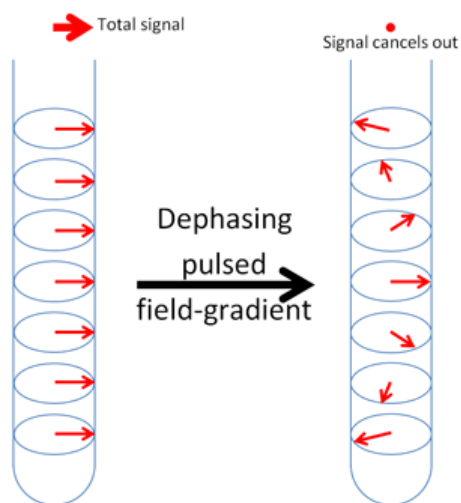


Figure 4.8: Application of a magnetic field gradient along z-axis. Image source: http://chem.ch.huji.ac.il/nmr/techniques/other/diff/diff_files/gradientpulse.gif

would want a magnetic field of the form:

$$\vec{B}(r) = B_0 \hat{e}_z$$

A magnetic field gradient is a spatially inhomogeneous magnetic field. For example,

$$\vec{B}(r) = B_0 \hat{e}_z + G_0 z \hat{e}_z$$

. Since the Larmour precession frequency of the nuclei is directly proportional to the magnetic field, the application of a field gradient will cause nuclei different at different spatial locations to precess with different precession frequencies. The result is that there will be no net transverse magnetization 4.8.

Torrey Oscillations

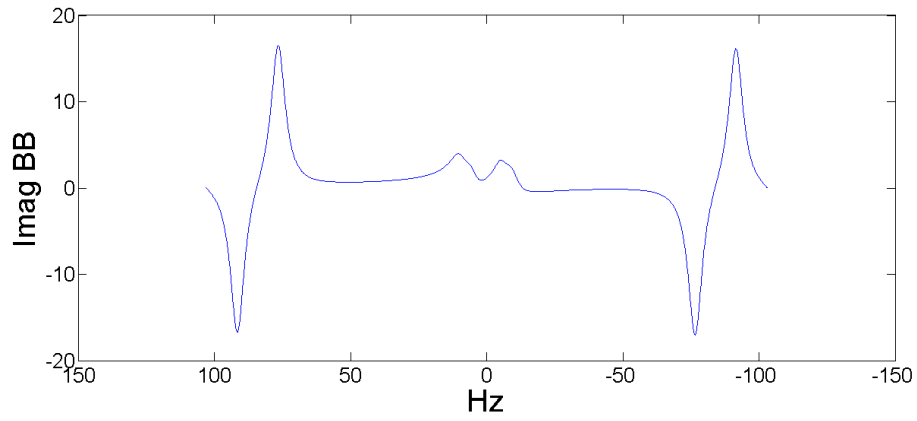
On applying a strong RF pulse along a direction perpendicular to the initial magnetization direction, the magnetization will start precessing about that axis in the rotating field of the RF pulse. Due to spatial RF field inhomogeneity which arises due to various reasons, the magnetization damps and gets suppressed (Torrey oscillations). In our experiment, we use this method to suppress proton magnetization(125 Hz power field for 2ms).

4.4 Results

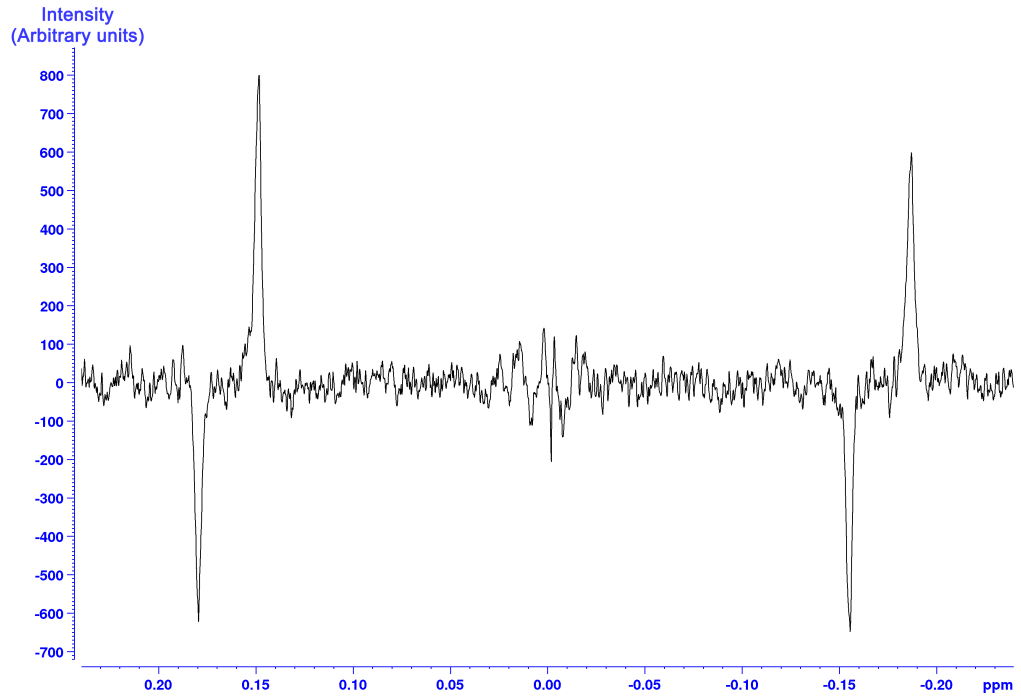
Here, we present the simulated and experimental spectra confirming the realization of the set of universal quantum gates for a two qubit system, described in 4.3. Here, we label the two proton qubits as 1,2 and the ^{13}C qubit as 3 and $I_{x,y,z} = \frac{1}{2}\sigma_{x,y,z}$.

4.4.1 CNOT gate

Starting from the initial state $\rho_{init} = I_y^1$, the CNOT gate was applied. The spectrum after the CNOT gate was found to match well with the simulated spectrum as shown in figure 4.9a.



(a) Simulated CNOT spectrum



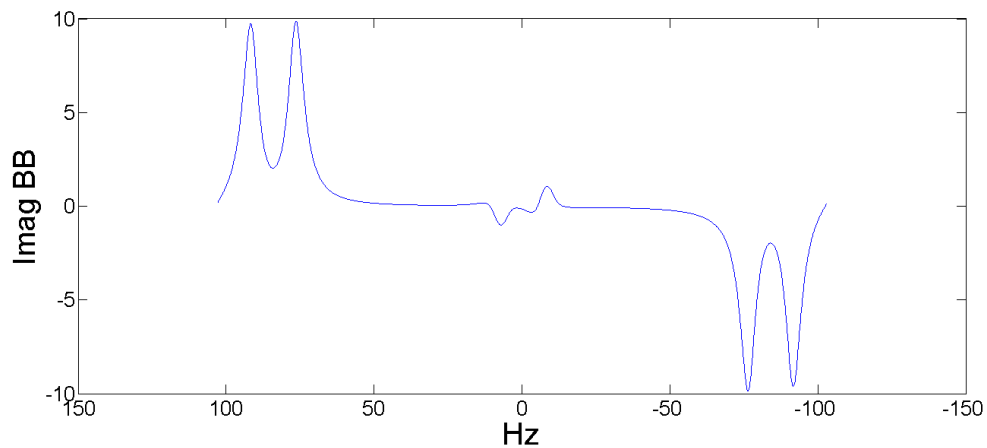
(b) Experimental CNOT spectrum

Figure 4.9: CNOT gate on H^1 , conditional on H^2

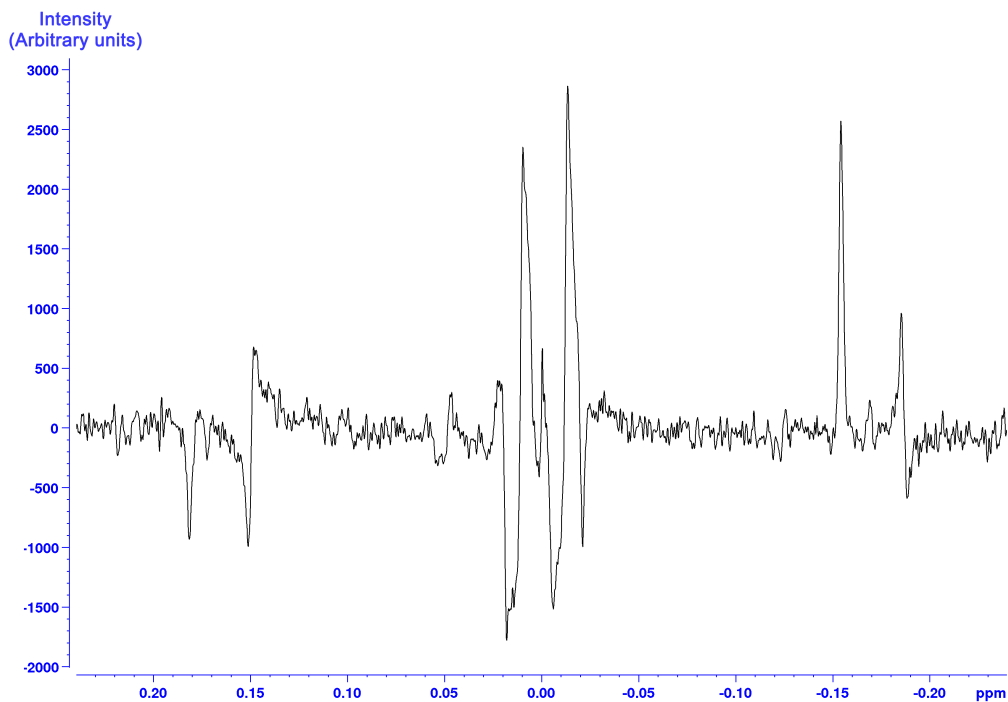
4.4.2 Hadamard gate

Starting from the initial state $\rho_{init} = I_y^1 I_z^3$, the Hadamard gate was applied on the first spin. The spectrum after applying the gate was found to match

well with the simulated spectrum (Imaginary part), the global phase of 180° being irrelevant.



(a) Simulated Hadamard spectrum

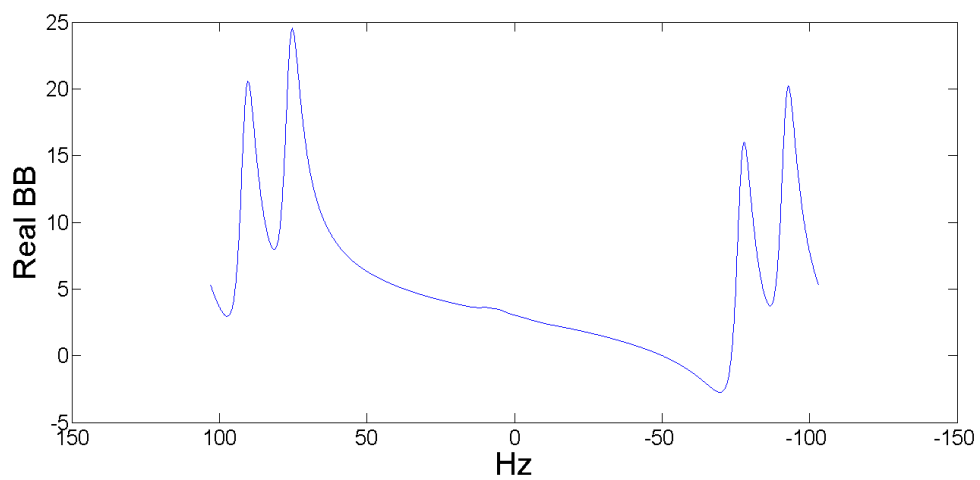


(b) Experimental Hadamard spectrum

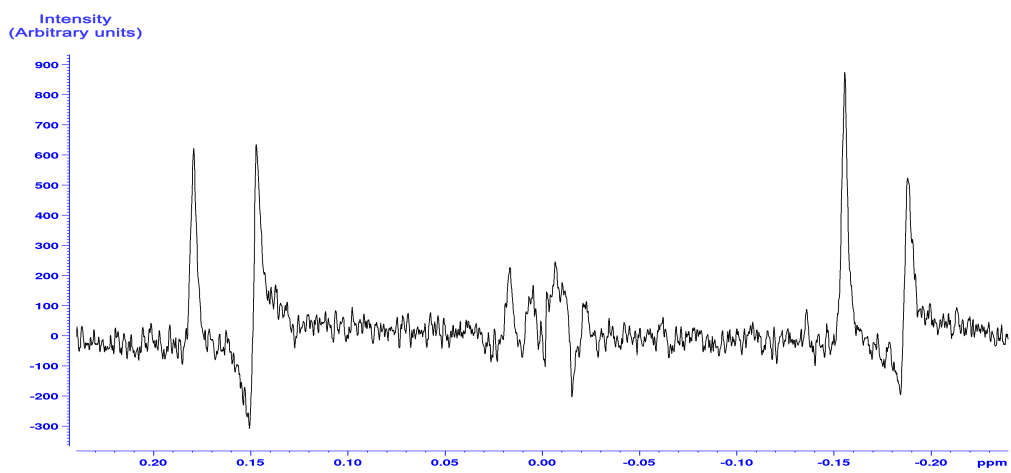
Figure 4.10: Hadamard gate on H^1

4.4.3 $\pi/8$ gate

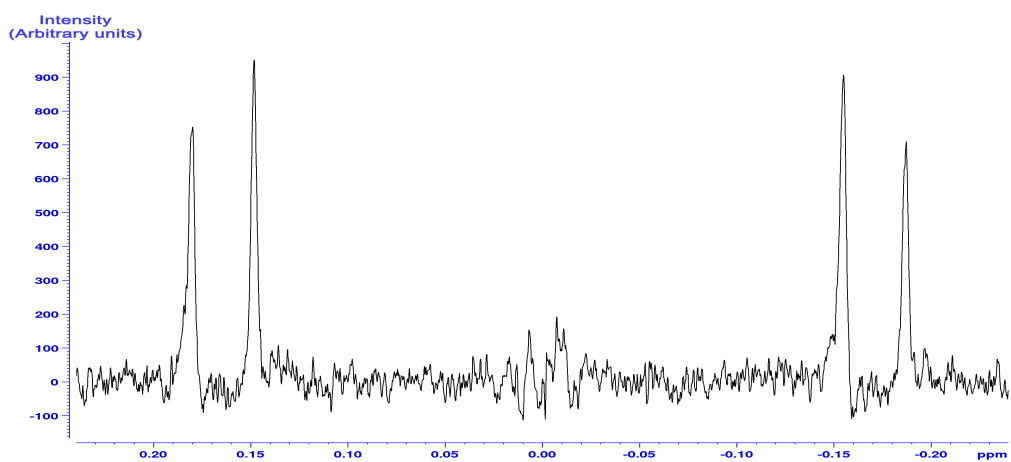
Starting from the initial state $\rho_{init} = I_x^1$, the phase gate was applied on the first spin. The spectrum after applying the gate was found to match fairly well with the simulated spectrum (Real part). There is more room for improvement in gate optimization. We can compare this to the signal from reference state $\rho_{init} = I_x^1$.



(a) $\pi/8$ gate simulated spectrum



(b) $\pi/8$ gate experimental spectrum



(c) $\pi/8$ gate reference spectrum

Figure 4.11: $\pi/8$ gate on H^1

4.5 Conclusion and Discussion

In this chapter, we demonstrated that it is possible to achieve universal control in a pair of effectively chemically equivalent qubits by means of actuator qubits. This may have important implications in implementing decoherence free subspaces, since unlike in usual cases, the use of equivalent qubits will enable the logical qubit to return completely to the decoherence free subspace after undergoing evolution under some control field. At the same time, we maintain full control, although indirectly, over the qubits by means of an actuator qubit. Furthermore, this approach may be relevant to many other qubit realizations such as spin qubits in quantum dots and electronic spins in silicon and diamond.

References

- [1] A. Einstein, B. Podolsky, N. Rosen, Can quantum-mechanical description of physical reality be considered complete?, *Phys. Rev.* 47 (1935) 777–780. doi:10.1103/PhysRev.47.777.
URL <http://link.aps.org/doi/10.1103/PhysRev.47.777>
- [2] E. Schrödinger, Die gegenwärtige Situation in der Quantenmechanik, *Naturwissenschaften* 23 (1935) 807–812. doi:10.1007/BF01491891.
- [3] M. Arndt, O. Nairz, J. Vos-Andreae, C. Keller, G. van der Zouw, A. Zeilinger, Wave-particle duality of c60 molecules, *Nature* 401 (6754) (1999) 680–682. doi:10.1038/44348.
URL <http://dx.doi.org/10.1038/44348>
- [4] *Decoherence and the Quantum-To-Classical Transition*, Springer Berlin Heidelberg, Berlin, Heidelberg, 2007, Ch. Introducing Decoherence, pp. 1–12. doi:10.1007/978-3-540-35775-9_1.
URL http://dx.doi.org/10.1007/978-3-540-35775-9_1
- [5] P. W. Shor, Polynomial-Time Algorithms for Prime Factorization and Discrete Logarithms on a Quantum Computer, *SIAM Review* 41 (2) (1999) 303–332.
URL <http://scitation.aip.org/getabs/servlet/GetabsServlet?prog=normal&id=SIREAD000041000002000303000001&idtype=cvips&gifs=yes>
- [6] L. K. Grover, A fast quantum mechanical algorithm for database search, in: *Proceedings of the Twenty-eighth Annual ACM Symposium on Theory of Computing, STOC '96*, ACM, New York, NY, USA, 1996, pp. 212–219. doi:10.1145/237814.237866.
URL <http://doi.acm.org/10.1145/237814.237866>
- [7] L. Viola, S. Lloyd, Dynamical suppression of decoherence in two-state quantum systems, *Phys. Rev. A* 58 (1998) 2733–2744. doi:10.1103/

PhysRevA.58.2733.

URL <http://link.aps.org/doi/10.1103/PhysRevA.58.2733>

- [8] L. Viola, E. Knill, S. Lloyd, Dynamical decoupling of open quantum systems, *Phys. Rev. Lett.* 82 (1999) 2417–2421. doi:10.1103/PhysRevLett.82.2417.
URL <http://link.aps.org/doi/10.1103/PhysRevLett.82.2417>
- [9] P. W. Shor, Scheme for reducing decoherence in quantum computer memory, *Phys. Rev. A* 52 (1995) R2493–R2496. doi:10.1103/PhysRevA.52.R2493.
URL <http://link.aps.org/doi/10.1103/PhysRevA.52.R2493>
- [10] D. A. Lidar, K. Birgitta Whaley, *Irreversible Quantum Dynamics*, Springer Berlin Heidelberg, Berlin, Heidelberg, 2003, Ch. Decoherence-Free Subspaces and Subsystems, pp. 83–120. doi:10.1007/3-540-44874-8_5.
URL http://dx.doi.org/10.1007/3-540-44874-8_5
- [11] G. Teklemariam, E. M. Fortunato, C. C. López, J. Emerson, J. P. Paz, T. F. Havel, D. G. Cory, Method for modeling decoherence on a quantum-information processor, *Phys. Rev. A* 67 (2003) 062316. doi:10.1103/PhysRevA.67.062316.
URL <http://link.aps.org/doi/10.1103/PhysRevA.67.062316>
- [12] G. Unnikrishnan. arXiv:1602.03026.
- [13] P. Cappellaro, J. S. Hodges, T. F. Havel, D. G. Cory, Principles of control for decoherence-free subsystems, *The Journal of Chemical Physics* 125 (4). doi:http://dx.doi.org/10.1063/1.2216702.
URL <http://scitation.aip.org/content/aip/journal/jcp/125/4/10.1063/1.2216702>
- [14] T. Yuge, S. Sasaki, Y. Hirayama, Measurement of the noise spectrum using a multiple-pulse sequence, *Phys. Rev. Lett.* 107 (2011) 170504. doi:10.1103/PhysRevLett.107.170504.
URL <http://link.aps.org/doi/10.1103/PhysRevLett.107.170504>
- [15] R. Sarkar, P. Ahuja, P. R. Vasos, A. Bornet, O. Wagnieres, G. Bodenhausen, Long-lived coherences for line-narrowing in high-field nmr, *Progress In Nuclear Magnetic Resonance Spectroscopy* 59 (EPFL-REVIEW-171250) (2011) 83–90.

- [16] M. Levitt, *Spin Dynamics: Basics of Nuclear Magnetic Resonance*, Wiley, 2001.
URL https://books.google.co.in/books?id=_1wZXxz1TIQC
- [17] Y. Kondo, M. Nakahara, S. Tanimura, S. Kitajima, C. Uchiyama, F. Shibata, Generation and suppression of decoherence in artificial environment for qubit system, *Journal of the Physical Society of Japan* 76 (7) (2007) 074002. arXiv:<http://dx.doi.org/10.1143/JPSJ.76.074002>, doi:10.1143/JPSJ.76.074002.
URL <http://dx.doi.org/10.1143/JPSJ.76.074002>
- [18] W. H. Zurek, Environment-induced superselection rules, *Phys. Rev. D* 26 (1982) 1862–1880. doi:10.1103/PhysRevD.26.1862.
URL <http://link.aps.org/doi/10.1103/PhysRevD.26.1862>
- [19] L. Viola, E. Knill, Random decoupling schemes for quantum dynamical control and error suppression, *Phys. Rev. Lett.* 94 (2005) 060502. doi:10.1103/PhysRevLett.94.060502.
URL <http://link.aps.org/doi/10.1103/PhysRevLett.94.060502>
- [20] S. Banerjee, C. M. Chandrashekar, A. K. Pati, Enhancement of geometric phase by frustration of decoherence: A parrondo-like effect, *Phys. Rev. A* 87 (2013) 042119. doi:10.1103/PhysRevA.87.042119.
URL <http://link.aps.org/doi/10.1103/PhysRevA.87.042119>
- [21] D. D’Alessandro, *Introduction to Quantum Control and Dynamics*, Chapman & Hall/CRC Applied Mathematics & Nonlinear Science, CRC Press, 2007.
URL <https://books.google.pt/books?id=e5M0id5enzQC>
- [22] D. Bacon, J. Kempe, D. A. Lidar, K. B. Whaley, Universal fault-tolerant quantum computation on decoherence-free subspaces, *Phys. Rev. Lett.* 85 (2000) 1758–1761. doi:10.1103/PhysRevLett.85.1758.
URL <http://link.aps.org/doi/10.1103/PhysRevLett.85.1758>
- [23] P. Cappellaro, J. S. Hodges, T. F. Havel, D. G. Cory, Control of qubits encoded in decoherence-free subspaces, *Laser Physics* 17 (4) 545–551. doi:10.1134/S1054660X0704038X.
URL <http://dx.doi.org/10.1134/S1054660X0704038X>
- [24] T. W. Borneman, C. E. Granade, D. G. Cory, Parallel information transfer in a multinode quantum information processor, *Phys. Rev. Lett.* 108 (2012) 140502. doi:10.1103/PhysRevLett.108.140502.
URL <http://link.aps.org/doi/10.1103/PhysRevLett.108.140502>

- [25] J. Zhang, D. Burgarth, R. Laflamme, D. Suter, Experimental implementation of quantum gates through actuator qubits, *Phys. Rev. A* 91 (2015) 012330. doi:10.1103/PhysRevA.91.012330.
URL <http://link.aps.org/doi/10.1103/PhysRevA.91.012330>
- [26] C. D. Aiello, P. Cappellaro, Time-optimal control by a quantum actuator, *Phys. Rev. A* 91 (2015) 042340. doi:10.1103/PhysRevA.91.042340.
URL <http://link.aps.org/doi/10.1103/PhysRevA.91.042340>
- [27] M. A. Nielsen, I. L. Chuang, *Quantum Computation and Quantum Information: 10th Anniversary Edition, 10th Edition*, Cambridge University Press, New York, NY, USA, 2011.
- [28] G. Bhole, V. Anjusha, T. MahesharXiv:1512.08385.